In situ Cosmogenic ^{10}Be and ^{26}Al Reveal the Complex Exposure and Erosion History of the Landscape Once Covered by the Quebec-Labrador Ice Dome

Peyton M. Cavnar[1,2], Paul R. Bierman[1,2], Jeremy D. Shakun[3], Lee B. Corbett[1], Danielle LeBlanc[3,7], Gillian L. Galford[1,2], Pierre-Olivier Couette[4,5], Jean-Francois Ghienne[5], Patrick Lajeunesse[4], Jérôme van der Woerd[5], and Marc Caffee[6]

[1]Rubenstein School for the Environment and Natural Resources, University of Vermont, Burlington, United States

[2]Gund Institute for the Environment, Burlington, United States

[3]Department of Earth and Environmental Sciences, Boston College, Chestnut Hill, United States

[4]Département de Géographie, Université Laval, Québec, Canada

[5]Institut Terre & Environnement de Strasbourg (ITES), UMR 7063, CNRS, Université de Strasbourg, Strasbourg, France

[6]PRIME Laboratory, Purdue University, West Lafayette, United States

[7]Woods Hole Oceanographic Institution, Falmouth, MA, United States

Correspondence to: Peyton M. Cavnar (cavnar.peyton@gmail.com) and Paul Bierman (pbierman@uvm.edu)

Abstract. The rate at which ice sheets erode rock and produce sediment is poorly known. Here, we use paired cosmogenic nuclides in both deglacial and modern sediment to understand better the efficacy with which the Quebec-Labrador Ice Dome (QLID) of the Laurentide Ice Sheet eroded bedrock and generated sand and boulders across the landscape of eastern Canada. We sampled deglacial sediment (esker and delta sand, n=10), sediment from modern streams (n=11), one bedrock outcrop, and a bedrock depth profile (n=7), measuring concentrations of ^{10}Be and ^{26}Al in quartz isolated from all samples. We also collated published cosmogenic nuclide measurements of boulders and bedrock from eastern Canada (n = 237 samples) and using estimates of deglaciation timing, calculated initial nuclide concentrations when the material was exposed by the most recent deglaciation, between 6.3 to 15.2 ka.

At the time of deposition, all 10 deglacial sand samples contained ^{10}Be and ^{26}Al, on average equivalent to several thousand years of surface exposure. The ubiquitous presence of ^{10}Be and ^{26}Al in eastern Quebec deglacial sediment is consistent with older-than-expected exposure ages for bedrock outcrops (n = 26 of 46 samples) and boulders (n = 65 of 192 samples) once covered by the QLID. Error-weighted averages of ^{26}Al/^{10}Be ratios for both deglacial (6.1±0.3, all uncertainties 1 SD) and modern sediment samples (6.6±0.5) are lower than the measured production ratio at high latitudes (Greenland, 7.3±0.3), suggesting cumulative burial of at least some sediment grains for at least hundreds of thousands of years.

This burial history suggests that ice at the middle of the QLID either survived some interglacials and/or that the average sediment residence time on the landscape is several times longer than a 100 ky glacial cycle, allowing storage and burial of sediment over multiple glacial cycles, either under ice and/or in thick deposits such as deltas

and moraines. Modern river sand contains on average only slightly higher nuclide concentrations than deglacial sediment, suggesting that river sand is predominately recycled from glacial deposits. Together, the new sediment data (which amalgamate across large areas of the landscape), and our compilation of bedrock and boulder point data, suggest that the average depth of bedrock erosion by ice and the speed of glacial sediment transport in eastern Canada were insufficient to remove material containing cosmogenic nuclides produced during prior interglacial(s).

1. Introduction

Ice sheets are important geomorphic agents of high-latitude landscape change (Patton et al., 2024; Sugden, 1978; Wilner et al., 2024) although the rates at which they erode landscapes and transport sediment are not well constrained. Available data suggest that both erosion and sediment transport rates are spatially and temporally variable (e.g., Alley et al., 2019; Cowton et al., 2012; Hallet et al., 1996; Patton et al., 2022). Rates of glacial erosion appear to be sensitive to the time-scale, making it difficult to accurately compare short-term, contemporary rates of glacial erosion and sediment export to those determined over longer time scales (Ganti et al., 2016; Wilner et al., 2024). Modelling sub-glacial processes, including rates of erosion and sediment transport, is not straightforward and results do not always match field evidence (e.g., Hildes et al., 2004).

During the Last Glacial Maximum (LGM), between 20-25 ka, the Laurentide Ice Sheet (LIS) covered most of Canada and the northern United States (Dalton et al., 2022). It was the largest body of ice in the Northern Hemisphere holding about 70 meters of sea level equivalent (Simms et al., 2019). Its ablation during the latest Pleistocene and early Holocene (characterized by collapse of northern Canadian ice domes) exposed a landscape that was once the ice sheet's bed including rocky outcrops shaped by abrasion and plucking, and deposits of glacial and post-glacial sediment (Occhietti et al., 2011). This relict landscape is an archive of past glacial and interglacial landscape behavior that can be used to untangle the history of landscape change (e.g., Bierman et al., 1999; Booth, 1994; Collins et al., 2024; Schaefer et al., 2016).

Quantitative geochronology techniques, primarily radiocarbon dating of organic material and cosmogenic nuclide exposure dating of bedrock and boulders, has established broad outlines of the post-LGM retreat history of the LIS (Dalton et al., 2023). Yet, uncertainties remain because dates from different chronometers do not always match and the concentrations of cosmogenic nuclides at the time of boulder and bedrock exposure and sediment deposition remain poorly constrained (Bierman et al., 1999, 2015; Briner et al., 2016; Halsted et al., 2024; Staiger et al., 2005). Paired nuclide cosmogenic burial dating has provided ages for pre-LGM LIS advances (Balco, 2005; Balco and Rovey, 2008, 2010).

Our study seeks to understand better the erosivity of LIS ice in eastern Canada by measuring and interpreting the concentrations of the cosmogenic nuclides ^{26}Al and ^{10}Be in sediment transported by the LIS. To accomplish this goal, we sampled along two transects stretching outward from the former middle of the Quebec-Labrador Ice Dome (QLID) at Labrador City: one eastward toward the Atlantic coast at Goose Bay, Labrador, and another southward to the St. Lawrence River near Quebec City (Figures 1 and 2). To provide context for our samples, we compiled published cosmogenic nuclide analyses of bedrock and glacially transported boulders from the QLID and used independent age estimates of deglaciation (Dalton et al., 2020) to estimate nuclide concentration at the time these sample sites were first exposed by LIS retreat.

The new data, and those we compiled, together allow us to constrain better the accuracy of cosmogenic exposure ages calculated for bedrock surfaces and erratic boulders in areas once covered by the QLID. Our work provides additional context for interpreting cosmogenic nuclide measurements made in sand-sized sediment of glacial and interglacial age present in marine sediment cores collected offshore of former and current ice sheets (e.g, Bierman et al., 2016; Christ et al., 2020; LeBlanc et al., 2023) as well sub-ice bedrock and sediment (Bierman et al., 2024a; Christ et al., 2021, 2023; Schaefer et al., 2016).

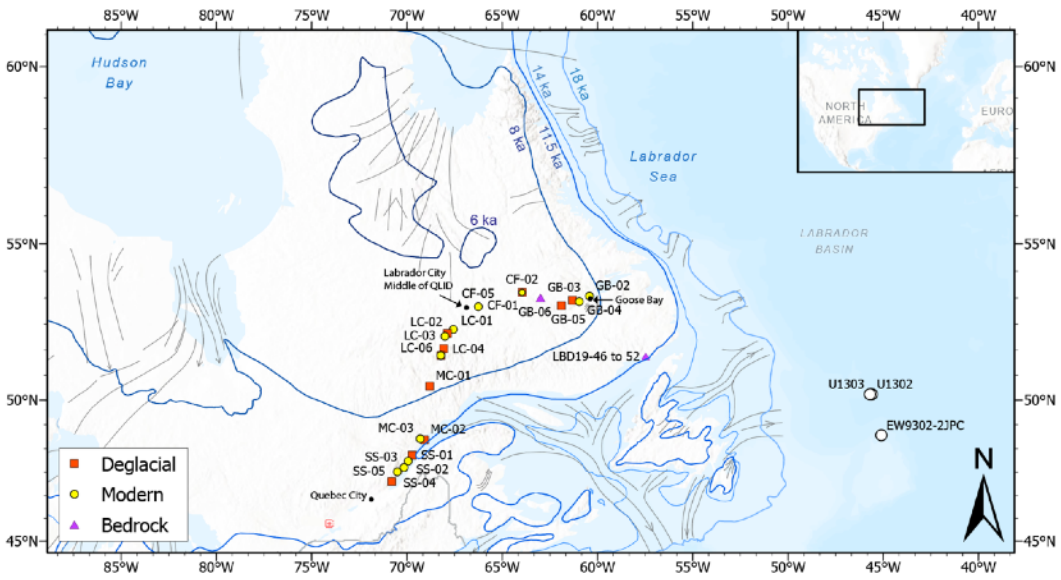

Figure 1. Map of field area with sample sites for new data included in this paper. Marine sediment cores with sample analyses in LeBlanc et al. (2023) shown by open circles. Terrestrial samples with new data provided in this paper shown with symbol color and shape corresponding to sample type. Inset indicates location of field area. Grey lines indicate direction of ice flow (Margold et al., 2018). Blue deglacial isochrons from Dalton et al. (2020).

2. Study Site

The QLID occupied the eastern subarctic Canadian Shield. The area we focus on is underlain mostly by Proterozoic quartzofeldspathic gneisses and granites (Hynes and Rivers, 2010). Regolith and soil are commonly thin and patchy (<2.5 m; Pelletier et al., 2016) and punctuated by prominent bedrock outcrops and glacial erratics (Ullman et al., 2016). Central and southern Quebec-Labrador also includes multiple moraine systems that mark and track the final deglaciation of the ice dome into the early Holocene (Couette et al., 2023; Occhietti et al., 2011; Ullman et al., 2016). There are eskers and ice contact deltas where the ice front, during deglaciation, met a body of standing water (Liverman, 1997; Storrar et al., 2013). The paraglacial landscape we consider here is still experiencing glacio-isostatic rebound, with the greatest net post-glacial rebound having occurred near James Bay and southern Hudson Bay (250-270 m; Lajeunesse and Allard, 2005; Lavoie et al., 2012), compared to ~100 m along coastal eastern Labrador (Andrews and Tyler, 2011).

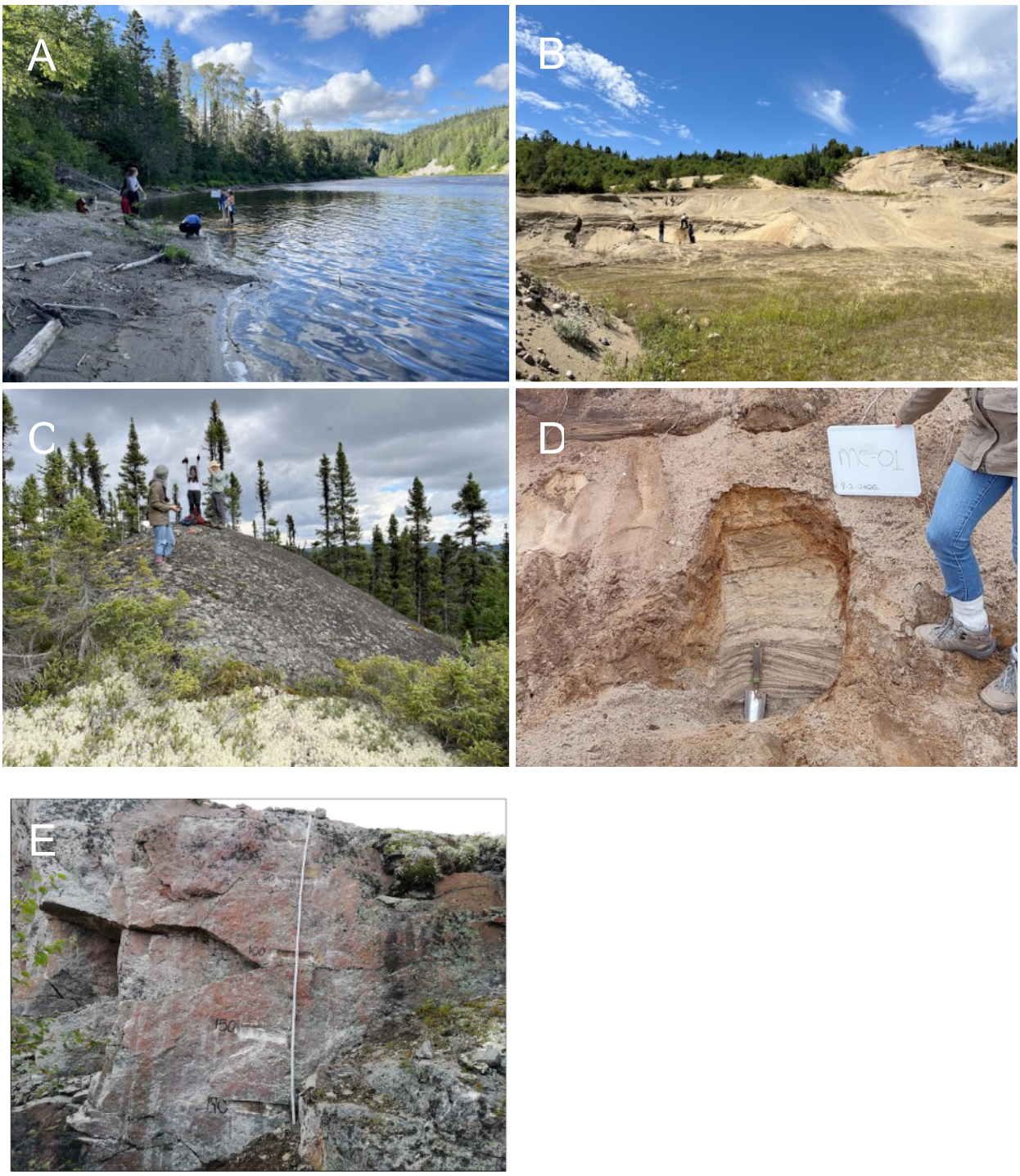

Figure 2. Photographs of representative field sites**.** A. Modern river sediment at MC-03. B. Deglacial sediment at SS-05. C. Bedrock outcrop at GB-06. D. Deglacial sediment at MC-01. E. Bedrock depth profile at LBD 19 46-52 exposed in roadcut after 1985. Depths in cm shown on outcrop. Note sample at 10 cm depth is offset to left of profile.

Eastern Canada is dominated by boreal spruce forests, sedges, and muskegs (shallow bogs covered in moss), a sub-arctic ecosystem prone to burning during dry periods in the summer, with a recorded fire history stretching back to the 1950's (Payette et al., 1989). Northern Quebec and Labrador are classified under the Dfc climate zone (cool continental climate/subarctic) according to the Köppen climate classification system (Amani et al., 2019; Beck et al., 2018). During winter, ground-based measurements record a mean of ~158 mm of snow water equivalent (SWE) for eastern Canadian boreal forests (Larue et al., 2017). The St. Lawrence River flows from southwest to northeast and is located southeast of the middle of the QLID. The Churchill River flows east from the former middle of the QLID, draining into the Atlantic Ocean.

3. Background and Unanswered Questions

3.1. Cosmogenic Nuclides as Recorders of Glacial History and Process

Since the late 1980s, measurement of cosmogenic nuclides, most commonly ^{10}Be and ^{26}Al extracted from quartz, has helped elucidate the Quaternary history of glaciated landscapes and the rate of glacial processes. These nuclides are produced by cosmic-ray interaction with target atoms at and near Earth's surface. Near the surface, neutron spallation production is dominant, but deeper in a profile (>2 m), muons dominate nuclide production at rates much lower than near the surface (c.f. Braucher et al., 2013).

^{10}Be and ^{26}Al are produced in both rock and glacially deposited sediment. Analysis of their concentrations can provide information about the timing of deglaciation (e.g., Corbett et al., 2011), the depth of glacial erosion (e.g., Briner et al., 2006; Miller et al., 2006; Stroeven et al., 2002), the persistence of glacial sediment on the landscape (e.g., Nelson et al., 2014), the thermal conditions at the bed (e.g., Staiger et al., 2006), and in the right setting, the limits on the extent and timing of sediment and rock burial by ice sheets (e.g., Bierman et al., 1999; Briner et al., 2006; Christ et al., 2021; Corbett et al., 2016b, c; Marsella et al., 2000; Miller et al., 2006; Schaefer et al., 2016). Measuring the concentrations of ^{10}Be and ^{26}Al in the same sample can reveal periods of burial during or after near-surface exposure (Klein et al., 1986) because the nuclides decay at different rates; their half-lives differ by a factor of two (~1.36 and ~0.73 My, respectively).

Cosmogenic nuclide measurements made in detrital sediment from contemporary paraglacial channels (Nelson et al., 2014) and glacial deposits (e.g., Bierman et al., 2016; Goehring et al., 2010), have been used to infer the concentration of nuclides inherited from prior periods of exposure, to interpret ice sheet basal processes (Corbett et al., 2021), and to infer sediment sourcing (e.g., Balco, 2005; Bierman et al., 2016; Fame et al., 2018; Nelson et al., 2014). Cosmogenic nuclide measurements in marine sediments and in material collected from the base of ice cores allow inference of glacial process, ice sheet history, and interglacial landscape exposure (Bierman et al., 2016, 2024a; Blard et al., 2023; Christ et al., 2020, 2021, 2023; Schaefer et al., 2016; Shakun et al., 2018).

When a landscape is covered by a thick layer of ice, such as the LIS, or if sediment is stored in deposits thick enough to largely attenuate cosmic-ray penetration, production of *in situ* ^{26}Al and ^{10}Be is diminished or stops. As nuclides produced during initial exposure decay, the ^{26}Al/^{10}Be ratio decreases (Bierman et al., 1999), a change

that is detectable after several hundred thousand years of burial (Granger, 2014; Granger and Muzikar, 2001). Re-exposure to cosmic rays at or near Earth's surface increases the $^{26}Al/^{10}Be$ ratio, given sufficient time it approaches the production ratio. However, if sediment remains buried meters below the surface during interglacial periods (such as in deglacial deltas, till sheets, and eskers or under ice), ^{26}Al and ^{10}Be concentrations and the $^{26}Al/^{10}Be$ at the time of deposition are preserved in whole (deep burial) or in part (shallow burial) (Bierman et al., 2016; Goehring et al., 2010; Nelson et al., 2014).

Concentrations of ^{10}Be and ^{26}Al in glacial sediment therefore reflect the history of that sediment and of the ice sheet that eroded and transported it over time (e.g., Bierman et al., 2016; Briner et al., 2016; Corbett et al., 2021; Goehring et al., 2010; Nelson et al., 2014). Analysis of sediment deposited by retreating ice sheets allows inferences about erosion and transport efficiency at and near the former or present ice sheet bed. Long interglacial exposures, thin sediment cover, and bedrock that is resistant to erosion will allow high concentrations of nuclides to accumulate – for example, in central North America (Balco, 2005). On the other hand, persistent ice cover, high rates and depths of glacial erosion, and efficient sediment transport by ice will lower nuclide concentrations in glacially derived sediment, such as in parts of Greenland (Corbett et al., 2021; Goehring et al., 2010; Nelson et al., 2014).

3.2. Uncertain Laurentide Ice Sheet History in Eastern Canada

For most of the last glaciation, the LIS was characterized by three major ice domes, regions of especially thick (~4 km in some places), outflowing ice: Foxe Baffin Dome, Keewatin Dome, and the QLID considered here (Stokes et al., 2012). Changes in LIS size are thought to have broadly tracked the marine oxygen isotope record, though uncertainties in ice volume and extent through time reflect the paucity of geologic constraints (Batchelor et al., 2019).

The extent and duration of ice cover in eastern Canada during the Pleistocene remains uncertain. For example, the majority of Canada may have been ice-covered, with the LIS reaching 70% of its LGM extent as early as Marine Isotope Stage (MIS) 5d (~110 ka) or not until MIS 4 (~60 ka) (Dalton et al., 2022). During subsequent retreat into MIS 3 (~45 ka), a combination of luminescence, ^{14}C, and cosmogenic nuclide (^{10}Be and ^{26}Al) dating, along with evidence of a marine incursion into Hudson Bay, was used to argue for deglaciation of the middle of the LIS (Dalton et al., 2019; Pico et al., 2018). Others disagreed, interpretating these ages differently and citing the timing of carbonate-rich Heinrich events H5 and H4 which indicate that an intact, marine-terminating Hudson Strait ice stream existed during MIS 3 (Gauthier et al., 2024; Hodder et al., 2023, 2024; Miller and Andrews, 2019). Recent measurements of cosmogenic nuclide concentrations in quartz-bearing ice rafted debris (IRD), sourced at least in part from LIS-generated icebergs, also suggest ice may have lingered in eastern Canada through many interglacial periods of the last My (LeBlanc et al., 2023). Evidence includes $^{26}Al/^{10}Be$ ratios (4.7±0.8) measured in glacial-marine sediment well below the high-latitude (Greenland) production value of 7.3±0.3 (Corbett et al., 2017). Such depressed ratios require long (>1 My) periods of burial (by ice, sediment, or water) throughout the Pleistocene.

Retreat of the LIS in Quebec and Labrador following the LGM is constrained by radiocarbon ages on post-glacial marine shells and lake organic material (Dalton et al., 2020; Dyke, 2004) as well as cosmogenic ages that are incorporated in Dalton et al. (2023), which we chose not to use here because of potential circularity because their retreat model includes cosmogenic exposure ages. Together, these data suggest that the initial retreat was gradual,

with the eastern margin pulling back slowly from the continental shelf and not reaching the modern coastline until ~11.5 ka (Figure 1). Retreat rate increased when Hudson Bay opened and the QLID separated from other sectors of the LIS after ~8.5 ka. The margin of the ice sheet then retreated rapidly toward the middle of the landmass, disappearing entirely by ~6 ka.

In situ produced cosmogenic nuclides have been used extensively to date retreat of the QLID after the LGM in Labrador and Quebec. Clark et al. (2003) report 27 measurements (including 2 replicates) of ^{10}Be on 21 boulders and 4 bedrock surfaces, concluding that ice left valleys in the Torngat Mountains of northeastern Labrador between 12.0 and 13.4 ka. Further south, Ullman et al. (2016) used ^{10}Be concentrations in 65 boulder samples to demonstrate that ice left eastern Labrador at 10.4 ka and the St. Lawrence coastline in southern Quebec at 9.2 ka, reaching the middle of the Quebec-Labrador landmass at 6.7 ka. Couette et al. (2023) interpreted 37 ^{10}Be exposure ages on boulders to represent five still-stands or re-advances of the eastern LIS margin as it retreated inland from the coast of eastern Labrador (~12.9 ka, ~11.5 ka, ~10.4 ka, ~9.3 ka, and ~8.4-8.2 ka). Carlson et al. (2007), using 13 boulder measurements, determined that deglaciation across central Quebec occurred rapidly between 8.0 and 6.8 ka. Along western Ungava Bay, Lefebvre−Fortier et al. (2024) obtained ^{10}Be ages on 14 boulders from five marine strandlines, which suggest north-to-south ice margin retreat from 8.9 to 7.9 ka. Dubé-Loubert et al. (2018, 2021) placed deglaciation between 8.6 and 8.0 ka south of Ungava Bay based on 30 boulder ages from glaciomarine and ice-dammed lake delta surfaces. In the same region of northeastern Labrador, Rice et al. (2019) ^{10}Be dated 8 bedrock and 2 boulder samples. Rejecting two much older ages, they report a range of ages from 9.8 to 6.2 ka.

Taken together, the cosmogenic data generally agree with Dalton et al.'s (2020) radiocarbon-based chronology of deglaciation in eastern Canada. The ^{10}Be ages show a pattern of radial ice margin retreat toward the middle of Quebec-Labrador. However, many of the cosmogenic nuclide studies in this region of eastern Canada (Clark et al., 2003; Couette et al., 2023; Dubé-Loubert et al., 2018, 2021; Marquette et al., 2004; Rice et al., 2019) identify some older-than-expected ^{10}Be ages, which they attribute to inheritance of cosmogenic nuclides from periods of prior exposure. Ullman et al. (2016) note that radiocarbon ages are less by centuries than the ^{10}Be ages along that study's transects across the western, eastern, and southern part of the former QLID. This discrepancy could represent the pervasive presence of a low concentration of nuclides inherited from an earlier near-surface exposure, a lag in revegetation after deglaciation (c.f., Halsted et al., 2024), and/or production rate calibration/ scaling errors. We consider such inheritance in detail in this paper.

3.3. Assessing the Erosivity of Ice Sheets

In some places, ice sheets erode their bed (Alley et al., 2019; Cowton et al., 2012) and in others, they preserve bed materials (Bierman et al., 2024b). Erosion is considered typical of warm-based ice, whereas bed preservation is thought to be common where ice is cold-based and frozen to the bed (e.g., Corbett et al., 2016b; Sugden, 1978). Data generally support these assumptions (Koppes et al., 2015), although stratigraphic observations clearly show that ice, both warm and cold-based, can leave older sediment outcrops intact. For example, field surveys in areas overrun by the LIS reveal weathered regolith (Goldthwait and Kruger, 1938) including the fossiliferous Eocene Brandon Lignite in Vermont (Tiffney, 1994). Much of this weathered material is in valleys where ice was warm-based, meaning that pre-glacial, poorly consolidated material has survived repeated LIS

advances in New England, south of the field area investigated here. Weathered saprolite is similarly preserved in southeastern Quebec (LaSalle et al., 1985). On Baffin Island, pre-LGM lake sediments remain in basins overrun by ice as does heavily weathered bedrock on which sit fresh, late-glacial erratic boulders (Bierman et al., 2001; Miller et al., 2022).

Other studies have found varying inherited concentrations of cosmogenic nuclides in boulders and bedrock sampled near and inside the former LGM margin of the LIS. They attributed higher-than-expected nuclide concentrations to boulder reworking and insufficiently deep surface erosion during the brief time the ice occupied areas near the ice margin (Balco et al., 2002; Balter-Kennedy et al., 2024; Barth et al., 2019; Colgan et al., 2002; Halsted et al., 2024). In the northeastern United States, Halsted et al. (2024) suggested that boulders on LIS terminal moraines contained concentrations of inherited ^{10}Be equivalent to 2-6 ka of surface exposure. Mountain summits in New England, which till deposits indicate were covered by LGM ice, also have samples with much higher than expected cosmogenic exposure ages (Bierman et al., 2015; Corbett et al., 2019; Davis et al., 2015; Koester et al., 2021). In south-central Wisconsin, near the LGM ice margin, three out of five bedrock outcrops sampled had concentrations of ^{10}Be and ^{26}Al many times higher than predicted based on radiocarbon dating (Colgan et al., 2002). In the Torngat Mountains of northern Labrador, measurements of ^{26}Al and ^{10}Be on bedrock sites and erratic boulders at mountain summits provide evidence of minimal erosion (<1.4 m Ma^{-1}) and thus large concentrations of inherited nuclides where cold-based ice was predominant before deglaciation (Staiger et al., 2005).

Significant inheritance of cosmogenic nuclides is observed in areas once occupied by other Northern Hemisphere ice sheets as well. Towards the center of the Scandinavian ice sheet (northeastern Sweden) there is evidence that bedrock outcrops and boulder fields have been preserved through many glacial cycles since the late Cenozoic (Stroeven et al., 2002). A compilation of 953 cosmogenic nuclide measurements made on samples collected within the former extent of the Fennoscandian Ice sheet, showed that nuclide inheritance was common in both bedrock outcrops and erratic boulders (Jansen et al., 2019).

There is also evidence of minimal erosion near the margin of the Cordilleran Ice Sheet, with 8 out of 23 bedrock samples on Whitbey Island having ^{36}Cl/Cl ratios suggesting inheritance of nuclides produced from prior interglacials (Briner and Swanson, 1998). In northwest Greenland, 8 of 28 sampled boulders had high concentrations of ^{10}Be and ^{26}Al along with low ^{26}Al/^{10}Be ratios indicative of burial, indicating minimal subglacial erosion over multiple interglacial and glacial periods when the ice was presumably cold-based (Corbett et al., 2016b). Along Greenland's western ice margin, most subglacial cobbles (72 out of 86) sampled by Corbett et al. (2021) had a low concentration of ^{10}Be (median = 1.0 x 10^3 atoms g^{-1}), indicative of deep subglacial erosion and/or minimal prior surface exposure. Nevertheless, a subset of samples had higher ^{10}Be concentrations (> 3 x 10^3 atoms g^{-1}, n = 14), suggesting sourcing from minimally eroded (cold-based?) regions of the ice sheet where bedrock and sediment retained some ^{10}Be produced during prior ice-free periods.

Previously-published cosmogenic nuclide concentrations measured in samples of bedrock, boulders, and sediment from the area covered by the QLID suggest a varied pattern of erosion. Some areas were deeply eroded while others show evidence for inherited ^{10}Be indicating insufficient subglacial erosion to eliminate near-surface-produced cosmogenic nuclides. For example, of the five boulders sampled by Couette et al. (2023) from the early Holocene Paradise Moraine in eastern Labrador, two have implausible ^{10}Be exposure ages >20 ka and the other three

implausibly date the Paradise Moraine as older than a margin further from the middle of the ice dome. Ullman et al. (2016) likewise found anomalously high ^{10}Be concentrations in 10 out of 65 boulders along transects stretching eastward and southward from the middle of the QLID to the coast. Marquette et al. (2004) sampled upland bedrock, felsenmeer, and erratics in the Torngat Mountains and analyzed both ^{10}Be and ^{26}Al, the concentrations of which suggested that non-erosive ice covered the highlands while erosive ice occupied the valleys, retreating between 11.6 and 13.6 ka. Rice et al. (2019) inferred variable erosion conditions across an ~100-km portion of northeastern Quebec based on factor-of-two variations in ^{10}Be abundances of bedrock and till samples. Only Carlson et al. (2007), who collected a 13-sample transect of boulders along a 650 km transect westward from Labrador to James Bay, found no significant inheritance.

3.4. Cosmogenic nuclides as sediment source tracers

Cosmogenic nuclides have been used to identify sediment sources for both modern and paleo ice sheets. For example, Nelson et al. (2014) sampled rivers in the deglaciated areas of coastal Greenland. They found ^{10}Be concentrations in sediment sourced from the ice sheet (6,500±4,100 atoms g^{-1}) were significantly lower than sediment sourced from deglaciated terrain (14,900±8,600 atoms g^{-1}). This difference can be explained by contrasting exposure histories. Outboard of the ice margin, ^{10}Be concentrations in sediment increased when exposed to cosmic radiation since Holocene deglaciation while concentrations remained low under the ice sheet where production of ^{10}Be was minimal. Nelson et al. (2014) found that sediment sourced from a mix of deglaciated and glaciated terrain had ^{10}Be concentrations much closer to those of the glacial than deglacial endmember. These results suggest that most sediment moving through river systems in Greenland's paraglacial landscape comes from under the ice sheet rather than the adjacent deglaciated terrain. In southwest Minnesota and eastern South Dakota, Balco (2005) used a similar approach to determine sediment sourcing in a part of the midwestern United States previously covered by the LIS. Rivers there carried sediment with ^{10}Be and ^{26}Al concentrations (~60,000 and 270,000 atoms g^{-1}, respectively) like that of the glacial sediment they sampled. Both materials had lower ^{26}Al/^{10}Be ratios lower (4.70±0.29) than at production (~6.8).

4. Methods

4.1 Field Methods

To constrain nuclide concentrations in materials deposited by the LIS, we sampled deglacial sediment deposits (n=10) including deltas and eskers (Table 1). We collected modern river sediment samples (n=11) from trunk streams (St. Lawrence and Churchill River) as well as smaller tributaries. We collected deglacial sediment from clean faces in gravel pits or along river bluffs from 2 to 30 m below the upper land surface to reduce the effect of Holocene nuclide production following deglaciation (Table 2). We used shovels to dig ~0.3 m into the side of the landform before collecting ~500 g of sand. Modern river sediment samples were collected along channels away from areas of recent disturbance.

We collected outcrop samples using a rock saw and chisels at two sites, one interior and one coastal. The interior sample is from an exposed outcrop on a glacially molded bedrock knob in the middle of our eastern transect.

This sample is close to Ullman et al. (2016) site CL3, in which two of five boulders they sampled contained what the authors interpreted as inherited nuclides from period(s) of prior near-surface exposure. The coastal location is a roadcut 4 km inboard of the Belles Amours Moraine at the northern tip of the Gulf of St. Lawrence, where we obtained 7 samples along a 1.9 m bedrock depth profile; the surface sample (LBD19-46) was reported previously by Couette et al. (2023).

Table 1. Sample Location and Type

Sample Name	Type	Latitude [a]	Longitude [a]	Elevation (m) [a]
CF-02	Glaciofluvial Delta	53.5077	-63.9545	167
LC-02	Esker	52.2011	-67.8722	537
LC-04	Ice Contact Fan	51.7102	-68.0719	440
LC-05	Ice Contact Fan	51.4881	-68.2192	391
MC-01	Esker	50.4748	-68.8101	500
MC-02	Glaciofluvial Delta	48.6452	-69.0854	10
GB-03	Glaciofluvial Delta	53.2572	-60.7848	36
GB-05	Esker	53.0922	-61.8920	402
SS-01	Glaciofluvial Delta	48.1030	-69.7213	10
SS-05	Glaciofluvial Delta	47.1669	-70.8047	307
CF-01	Modern River Sediment	53.5060	-63.9585	126
CF-05	Modern River Sediment	53.0595	-66.2555	527
LC-01	Modern River Sediment	52.3365	-67.5671	533
LC-03	Modern River Sediment	52.1107	-68.0073	645
LC-06	Modern River Sediment	51.4882	-68.2229	401
GB-02	Modern River Sediment	53.3934	-60.4229	2
GB-04	Modern River Sediment	53.2201	-60.9549	210
MC-03	Modern River Sediment	48.6779	-69.3045	61
SS-02	Modern River Sediment	47.8942	-69.9368	128
SS-03	Modern River Sediment	47.6665	-70.1589	3
SS-04	Modern River Sediment	47.5157	-70.5066	25
GB-06	Bedrock	53.3351	-62.9912	484
LBD19-46 to LBD19-52	Bedrock Depth Profile	51.4780	-57.4756	75

[a] Location and elevation were measured in the field using a Garmin eTrex 20 GPS

4.2 Laboratory Methods

4.2.1 University of Vermont

To isolate and purify quartz for cosmogenic nuclide analysis at the University of Vermont (all sediment samples and the surface bedrock sample) we used a series of physical and chemical processes (Kohl and Nishiizumi, 1992) after sieving material to between 250 and 850 µm. We performed two 24-hour 6 N hydrochloric acid (HCl) etches in heated ultrasonic baths to remove grain coatings. We then used dilute (1%) hydrofluoric (HF) and nitric acid (HNO_3) etches for three 24-hour periods after which we sonicated samples in 0.5% HF and HNO_3 for a minimum of two weeks. We evaluated the purity of etched samples using inductively coupled plasma optical emission spectrometry (ICP-OES) after which impure samples were re-etched until each was sufficiently pure.

We extracted Be and Al from the purified quartz samples (17.3 – 22.2 g, n = 22) in the National Science Foundation/University of Vermont Community Cosmogenic Facility using methods described in Corbett et al. (2016a). Samples were prepared in two separate batches, each of which included a fully processed blank. We spiked the samples with ~250 µg ^{9}Be using a beryl carrier made in the Community Cosmogenic Facility with a Be concentration of 348 µg mL^{-1} (Table 3). We spiked samples with SPEX ICP Al standard (1000 ppm) as needed based on their quantity of native Al, ensuring at least 1500 µg of total Al in every sample. We quantified total Al in the samples by ICP-OES immediately following sample digestion. Following standard procedures (Corbett et al., 2016a), we removed replicate aliquots from the samples by mass (representing ~2% and ~4% of the sample, respectively), added 25 µL H_2SO_4 to each, evaporated the HF, then diluted the residual H_2SO_4 droplets by mass with a 0.25% H_2SO_4 solution spiked with Y as an internal standard.

Purdue Rare Isotope Measurement Laboratory performed accelerator mass spectrometry analysis (AMS). For $^{10}Be/^{9}Be$, measured ratios were normalized to primary standard 07KNSTD3110 with a ratio of 2.850 x 10^{-12} (Nishiizumi et al., 2007). For $^{26}Al/^{27}Al$, analyses were normalized to primary standard KNSTD with a ratio of 1.818 x 10^{-12} (Nishiizumi, 2004).

We used the known concentration of ^{9}Be added as carrier, along with the measured isotopic ratio and quartz mass, to calculate the concentration of ^{10}Be in each sample. Because of the native ^{27}Al within the samples, the concentration of ^{27}Al measured using ICP-OES after quartz dissolution was used to calculate the concentration of ^{26}Al. We subtracted the mean extraction process blank ratios of $^{10}Be/^{9}Be$ ((7.41±2.81) x 10^{-16}; n = 2) and $^{26}Al/^{27}Al$ ((5.39±0.71) x 10^{-16}; n = 2) from the measured ratios and propagated the uncertainty in quadrature (Table 3).

4.2.2 University of Strasbourg

To isolate and purify quartz for cosmogenic nuclide analysis at the University of Strasbourg, Institut Terre et Environnement de Strasbourg (7 bedrock profile samples, LBD19-46 to 52) we used a series of physical and chemical processes (Bierman et al., 2002; Kohl and Nishiizumi, 1992). We sieved material to between 250 and 1000 µm. For each sample, we performed a 12-hour 6 N HCl leaching to eliminate oxides and organic material. Magnetic minerals were then separated with a Frantz magnetic separator. We used dilute (1%) HF and HNO_3 acid etches in ultrasonic baths for five 12-hour periods. We evaluated the purity of etched samples using inductively coupled plasma optical emission spectroscopy (ICP-OES) after which impure samples were re-etched until each was sufficiently pure.

We extracted Be and Al from the purified quartz samples (27.02 – 56.99 g, n = 7) in the cosmogenic nuclide laboratory at the University of Strasbourg following a protocol modified from Kohl and Nishiizumi (1992). Samples were prepared together with a fully processed blank. We spiked the samples with ~250 or ~500 µg ^{9}Be using a Scharlab ICP 1000 mg/l Be standard. We spiked only the blank with a Scharlab ICP 1000 mg/l Al standard as the quantity of native Al was sufficient in every sample. We quantified total Al in the samples by ICP-OES following sample digestion and three successive fuming steps with 2 to 4 ml of perchloric acid ($HClO_4$). Be and Al were isolated through anion and cation exchange columns and precipitated as hydroxides. They were then dried and calcinated to BeO and AlO at 750°C.

AMS analysis was performed at ASTER, the French National Laboratory of Cosmogenic Nuclides in CEREGE (Aix-en-Provence). For ^{10}Be/^{9}Be, measured ratios were normalized to in-house CEREGE standard STD-11 with an assumed ratio of (1.191±0.013) × 10^{-11} (Braucher et al., 2015). For ^{26}Al/^{27}Al, analyses were normalized to in-house CEREGE standard SM-AL-11 with a ratio of (7.401±0.064) x 10^{-12} (Merchel and Bremser, 2004).

We used the known concentration of ^{9}Be added as carrier, along with the measured isotopic ratio and quartz mass to calculate the concentration of ^{10}Be in each sample. Because of the native ^{27}Al within the samples, the concentration of ^{27}Al measured using ICP-OES after quartz dissolution was used to calculate the concentration of ^{26}Al. We subtracted the extraction process blank ratios of ^{10}Be/^{9}Be ((5.21±0.42) x 10^{-15}) and ^{26}Al/^{27}Al ((6.25±6.25) x 10^{-16}) from the measured ratios and propagated the uncertainty in quadrature.

4.3 Statistical Analysis

We use the same value (alpha = 0.05) for all statistical tests we performed. We used both Wilcoxon rank-sum tests (due to the non-normal distribution of nuclide concentrations in modern sediment samples) and Tukey HSD tests to investigate significant differences between sample groups. We used a 2-standard deviation threshold for detectability; that is, if twice the analytical uncertainty exceeded the measured ratio, then we considered the sample to be below detection limits. This provides a 95% confidence that the isotopic ratios and concentrations we report are finite.

4.4 Data Compilation

To expand our assessment of cosmogenic nuclide concentrations in materials influenced by the QLID, we estimated the concentration of inherited nuclides present in published ^{10}Be data generated from samples of boulders and bedrock collected in the region by others. We obtained data from 200 samples (42 bedrock, 158 boulders) from Dalton et al.'s, (2023) North American ^{10}Be compilation and recalculated all ages with the online exposure calculator formerly known as CRONUS (Balco et al., 2008) (constant production rate model, version 3.0.2, constants 2024-08-26) using the global production rate and LSDn scaling (Lifton et al., 2014), accounting for differences in standardizations. We also included 37 ^{10}Be ages (3 bedrock, 34 boulders) from Couette et al. (2023) that were not in the Dalton et al. (2023) compilation and our one surface bedrock sample, following the same protocol.

4.5 Holocene Exposure Correction

For deglacial sediment samples and the single inland bedrock sample, we calculated the concentration of nuclides attributable to Holocene exposure. We used the online exposure age calculator (constant global production rate model, version 2.3) to determine the surface production rate (atoms g^{-1} yr^{-1}) of ^{10}Be and ^{26}Al for both muons (P_μ) and spallation (P_s) at each sample site (Balco et al., 2008). The production rate at depth was then estimated using an attenuation length of 165 g cm^{-2} for spallation (Λ_s) and 1400 g cm^{-2} for muons (Λ_μ). We validated the apparent muonogenic attenuation factor using the CRONUS implementation of Heisinger et al., (2002) (code P_mu_total.m) for sea level— yielding < 1% difference from our original calculations. We estimated uncertainties in the concentration of nuclides produced during the Holocene due to uncertainties in our sample depths and combined these in quadrature with AMS measurement uncertainties (Table 2). For sediment, we assumed a density (ρ) of 1.7 g/cm^3.

After establishing the nuclide production rate at depth, we calculated (using equation 1) the production since deglaciation (A in yr) of ^{10}Be and ^{26}Al (H in atoms g^{-1}) at the depth we collected each sample (D in cm), taking deglaciation age estimates for each sample site from Dalton et al. (2020) using radiocarbon-based LIS margin isochrons. For the rock sample, we used half the sample thickness (thickness = 2 cm) as the depth. Dalton 2020 gives isochrons in our study area for 6.3, 6.8, 7.3, 7.9, 8.1, 8.5, 8.7, 8.8, 9, 9.6, 10.3, 10.9, 11, 11.5, 11.8, 12.1, 12.8, 13.5, 14.2, and 14.9 cal ka. Thus, the resolution of the isochrons ranges from 100 to 700 years and averages 500 years. For samples located between isochrons, we estimated their deglaciation ages by linearly interpolating between the isochrons. Thus, typical uncertainties on our estimated deglaciation ages are likely a few centuries.

$$H = P_s \cdot 1/exp(\frac{D \cdot \rho}{\Lambda_s}) \cdot A + P_\mu \cdot 1/exp(\frac{D \cdot \rho}{\Lambda_\mu}) \cdot A \quad (1)$$

We subtracted the concentration of nuclides produced after deglaciation from the sample's measured ^{10}Be concentration to calculate the concentration of nuclides inherited at the time of deglaciation. We did not use the more recent reconstruction of LIS retreat from Dalton et al. (2023) to determine deglaciation ages because it incorporates updates based on the ^{10}Be data and thus risks circularity. We estimated the amount of inheritance in our coastal bedrock depth profile by fitting a production profile to the data representing 11.5 ky of exposure (the age of the adjacent Belles Amours Moraine; Couette et al. 2023) with varying concentrations of uniformly distributed inherited nuclides.

Table 2. Calculations for Holocene Exposure-Corrected Concentrations

Sample Name	Age (yr)[a]	Sample Depth (cm)[b]	Depth Uncertainty (cm)[b]	^{10}Be Muon Production Rate (atoms g^{-1} y^{-1})[c]	^{26}Al Muon Production Rate (atoms g^{-1}	^{10}Be Spallation Rate (atoms g^{-1} y^{-1})[c]	^{26}Al Spallation Rate (atoms g^{-1} y^{-1})[c]	Total ^{10}Be production rate at depth (atoms g^{-1} y^{-1})[d]	Total ^{26}Al production rate at depth (atoms g^{-1} y^{-1})[d]	^{10}Be correction (%)
CF-02	8000	800	-200, +200	0.081	0.743	5.02	33.85	0.032	0.290	1

LC-02	7800	250	-50, +50	0.092	0.854	7.13	48.08	0.611	4.289	20
LC-04	7900	200	-50, +50	0.089	0.823	6.50	43.83	0.898	6.229	34
LC-05	7700	250	-50, +50	0.087	0.807	6.20	41.81	0.536	3.777	15
MC-01	8600	180	-30, +20	0.091	0.841	6.84	46.14	1.144	7.898	53
MC-02	12400	2000	-200, +200	0.076	0.695	4.15	27.97	0.007	0.061	0
GB-03	8400	700	-200, +200	0.077	0.708	4.40	29.67	0.036	0.325	4
GB-05	8300	300	-100, +100	0.088	0.815	6.36	42.89	0.350	2.516	13
SS-01	12300	550	-150, +50	0.076	0.694	4.12	27.77	0.053	0.452	6
SS-05	12800	3000	-500, +500	0.084	0.777	5.48	36.94	0.002	0.020	0
GB-06	8100	1	0	0.090	0.838	6.75	45.55	6.840	46.388	71

[a]Deglaciation ages estimated based on proximity to deglacial isochrons in Dalton et al. (2020)

[b]Sample depth estimated in the field. Depth uncertainty estimated from photos and considered 95% confidence interval.

[c]Muon and spallation surface production rates estimated from the online calculator formerly known as CRONUS v2.3 (Balco et al., 2008)

[d]Total nuclide production rate at sample depth includes production from both muons and spallation, and assumes an attenuation length of 165 g cm^{-2} for spallation, 1400 g cm^{-2} for muons, and a sediment density of 1.7 g cm^{-3}. We applied no snow shielding correction.

5. Results

^{10}Be and ^{26}Al were above detection limit in all 8 bedrock samples and 21 of 22 sediment samples we analyzed, the one exception being the ^{26}Al measurement for sample GB-04, a modern stream sample (Table 3, Figure 3). For both nuclides, the average concentration is higher in the modern sediment ($3.31\pm1.57 \times 10^4$ ^{10}Be atoms g^{-1}, $2.12\pm1.18 \times 10^5$ ^{26}Al atoms g^{-1}) than in the deglacial sediment ($2.25\pm1.30 \times 10^4$ ^{10}Be atoms g^{-1}, $1.47\pm0.94 \times 10^5$ ^{26}Al atoms g^{-1}) but these differences are not statistically significant.

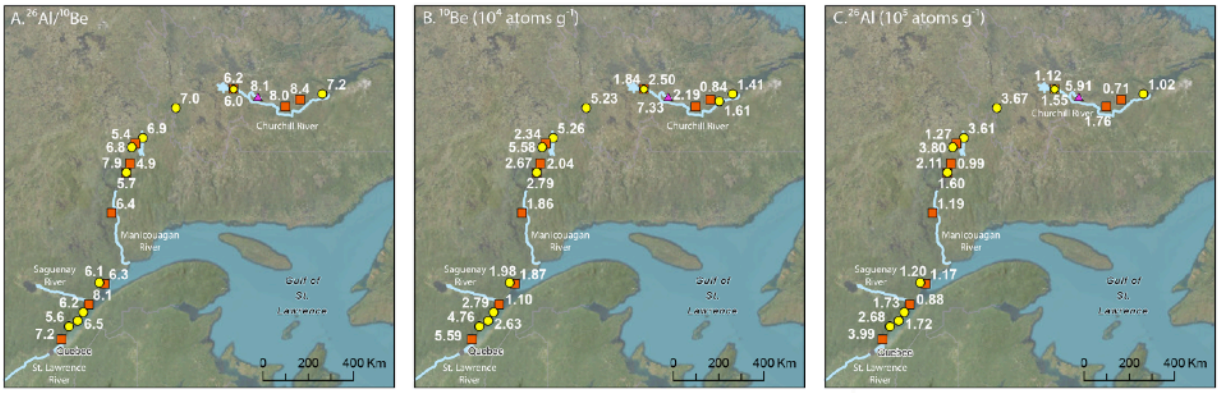

Figure 3. Maps showing new isotopic data excluding bedrock depth profile. A. $^{26}Al/^{10}Be$ ratio (n=21). B. Measured concentration of ^{10}Be (n=22). C. Measured concentration of ^{26}Al (n=21). Data in Table 3. Sample names and key as in Figure 1.

Table 3. Blank-Corrected Isotopic Data

Sample Name	Type	^{10}Be (atoms g^{-1})	^{10}Be Uncertainty (atoms g^{-1})	^{26}Al (atoms g^{-1})	^{26}Al Uncertainty (atoms g^{-1})	$^{26}Al/^{10}Be$	$^{26}Al/^{10}Be$ Uncertainty
CF-02	Deglacial	1.84×10^4	1.30×10^3	1.12×10^5	1.08×10^4	6.05	0.72
LC-02	Deglacial	2.34×10^4	1.45×10^3	1.27×10^5	1.07×10^4	5.44	0.57
LC-04	Deglacial	2.04×10^4	1.34×10^3	9.94×10^4	1.02×10^4	4.89	0.60
LC-05	Deglacial	2.79×10^4	1.88×10^3	1.60×10^5	1.67×10^4	5.72	0.71
MC-01	Deglacial	1.86×10^4	1.61×10^3	1.19×10^5	1.43×10^4	6.38	0.95
MC-02	Deglacial	1.87×10^4	1.54×10^3	1.17×10^5	9.56×10^3	6.27	0.73
GB-03	Deglacial	8.42×10^3	1.68×10^3	7.11×10^4	3.23×10^4	8.44	4.19
GB-05	Deglacial	2.19×10^4	1.99×10^3	1.76×10^5	2.23×10^4	8.02	1.25
SS-01	Deglacial	1.10×10^4	1.29×10^3	8.84×10^4	7.98×10^3	8.05	1.19
SS-05	Deglacial	5.59×10^4	2.63×10^3	3.99×10^5	2.81×10^4	7.15	0.61
CF-01	Modern	2.50×10^4	2.17×10^3	1.55×10^5	1.63×10^4	6.22	0.85
CF-05	Modern	5.23×10^4	2.18×10^3	3.67×10^5	2.32×10^4	7.02	0.53
LC-01	Modern	5.26×10^4	2.33×10^3	3.61×10^5	1.85×10^4	6.86	0.47
LC-03	Modern	5.58×10^4	2.41×10^3	3.80×10^5	2.38×10^4	6.82	0.52
LC-06	Modern	2.67×10^4	2.12×10^3	2.11×10^5	1.84×10^4	7.92	0.93
GB-02	Modern	1.41×10^4	1.41×10^3	1.02×10^5	3.46×10^4	7.24	2.56

GB-04	Modern	1.61×10^4	1.39×10^3	Below Detection Limit		----	----
MC-03	Modern	1.98×10^4	1.66×10^3	1.20×10^5	1.19×10^4	6.06	0.79
SS-02	Modern	2.79×10^4	2.01×10^3	1.73×10^5	1.25×10^4	6.19	0.63
SS-03	Modern	2.63×10^4	1.78×10^3	1.72×10^5	1.31×10^4	6.55	0.67
SS-04	Modern	4.76×10^4	2.16×10^3	2.68×10^5	3.51×10^4	5.64	0.78
GB-06	Bedrock	7.33×10^4	3.90×10^3	5.91×10^5	2.90×10^4	8.05	0.58
LBD19-46 (0 cm)	Bedrock	5.02×10^4	1.87×10^3	3.30×10^5	1.37×10^4	6.57	0.37
LBD19-47 (10 cm)	Bedrock	3.89×10^4	1.76×10^3	2.49×10^5	1.32×10^4	6.41	0.43
LBD19-48 (20 cm)	Bedrock	4.36×10^4	2.89×10^3	2.51×10^5	1.86×10^4	5.77	0.55
LBD19-49 (50 cm)	Bedrock	2.48×10^4	1.83×10^3	1.57×10^5	9.49×10^3	6.34	0.58
LBD19-50 (100	Bedrock	1.31×10^4	1.16×10^3	8.24×10^4	5.25×10^3	6.27	0.63
LBD19-51 (150	Bedrock	7.24×10^3	7.07×10^2	5.68×10^4	5.09×10^3	7.85	0.92
LBD19-52 (190	Bedrock	5.94×10^3	6.07×10^2	3.51×10^4	4.35×10^3	5.90	0.85

Nuclide concentrations and uncertainties incorporate blank corrections. Uncertainties are 1σ.
Depths of samples LBD19-46 to LBD19-52 in bedrock depth profile are given after sample name.

The bedrock sample (GB-06) had the highest concentration of ^{10}Be (7.33±0.39 x 10^4 atoms g^{-1}) and ^{26}Al (5.91±0.29 x 10^5 atoms g^{-1}) that we measured. The coastal bedrock depth profile had a surface concentration of 5.02±0.19 x 10^4 ^{10}Be atoms g^{-1} and 3.30±0.14 x 10^5 ^{26}Al atoms g^{-1} (Figure 4). Concentrations of both nuclides decrease exponentially with depth in the bedrock profile, with e-folding lengths of approximately 175 to 190 g cm^{-2}, longer than would be expected from spallation production alone (165 g cm^{-2}). We note that the sample at depth 10 cm does not fit well on the profile. It was taken to the left side of the other samples (Figure 2E) and may have had a different cover history.

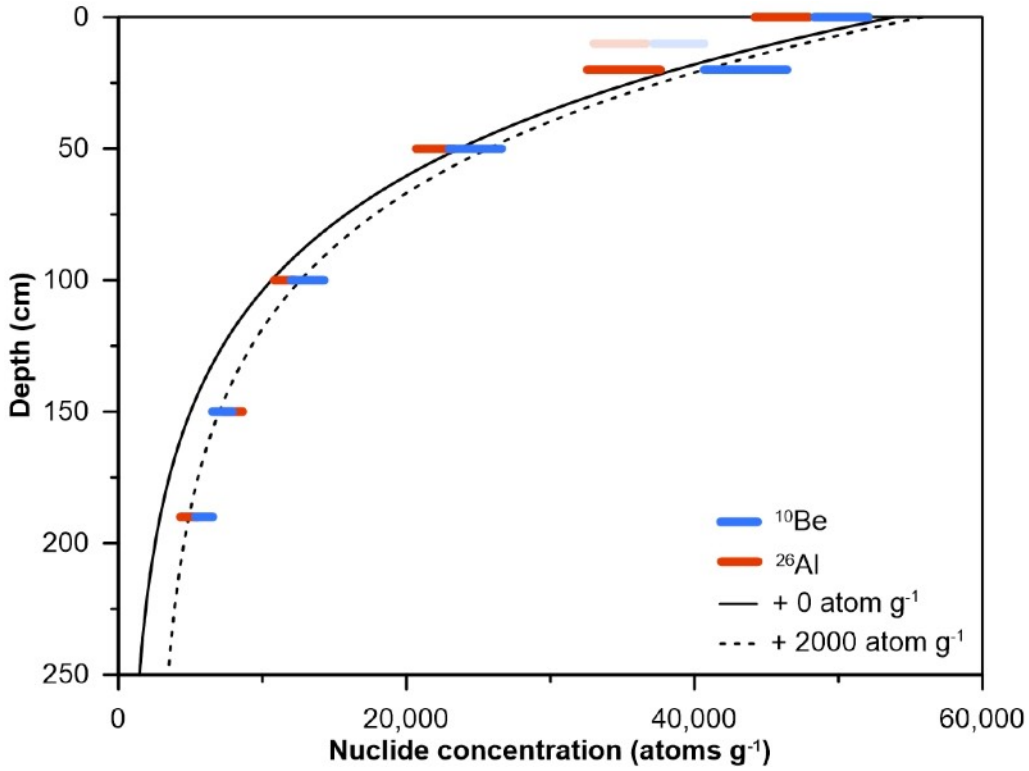

Figure 4. Depth profile in bedrock (sample set LBD-19, 46-52) with modelled fit for 11.5 kyr of surface exposure and inheritance of 0 and 2000 atoms g^{-1}. Symbols extend to 1 standard deviation analytic uncertainty. Solid line is fit with no inherited nuclides. Dashed line assumes uniform 2000 atoms g^{-1} inheritance for ^{10}Be. ^{26}Al was scaled to equivalent ^{10}Be concentration assuming $^{26}Al/^{10}Be$ ratio of 7.3. Shaded sample collected to the left of the profile (Figure 2E) and not considered in fit.

5.1. ^{10}Be and ^{26}Al Concentrations in Deglacial Samples Corrected for Holocene Exposure

After correcting for Holocene exposure, there is significant difference between the concentration of ^{10}Be in deglacial (mean, 1SD, n=10; 1.95±1.38 x 10^4 atoms g^{-1}) and modern (n=11, 3.31±1.57 x 10^4 atoms g^{-1}) sediment samples (p = 0.02) (Table 4, Figure 5A). For ^{26}Al, the concentration of deglacial (1.25±1.02 x 10^5 atoms g^{-1}) and modern (2.12±1.18 x 10^5 atoms g^{-1}) samples are also significantly different (p = 0.04) (Figure 5B). The modern samples are more variable in ^{10}Be concentration, with an interquartile range (IQR) of 2.76 x 10^4 atoms g^{-1} compared to the IQR of 7.85 x 10^3 atoms g^{-1} for Holocene exposure-corrected deglacial samples.

Both the bedrock sample (GB-06) and the bedrock depth profile (LBD19-46-52) contain nuclides inherited from prior exposure. Inferring an exposure age of 8.1 ky from maps of Dalton et al. (2020), and correcting for Holocene exposure with no erosion (the outcrop is smooth and rounded, Figure 2C), GB-06 contains 1.79 x 10^4 atoms g^{-1} of inherited ^{10}Be and 2.15 x 10^5 atoms g^{-1} of inherited ^{26}Al. Nuclide profiles, modelled to reflect Holocene exposure, best fit the bedrock profile data when they include ~2 x 10^3 atoms g^{-1} of inherited ^{10}Be and ~1.4 x 10^4 atoms g^{-1} of inherited ^{26}Al (Figure 4).

Our analysis of previously published ^{10}Be data suggests that inheritance of cosmogenic nuclides from prior period(s) of exposure is common in Quebec and Labrador. Over half of bedrock samples (n = 26 of 46, including our new sample GB-06) and a third of boulder samples (n = 65 of 192) contain significant concentrations of inherited nuclides, which we consider >3 x 10^3 atoms g^{-1} because that is the median analytical uncertainty in the dataset. The mean and range of inherited nuclide concentrations are larger for samples of bedrock (mean = 1.21 x 10^5 atoms g^{-1}; IQR = 8.04 x 10^4 atoms g^{-1}) than boulders (mean = 1.40 x 10^4 atoms g^{-1}; IQR = 1.28 x 10^4 atoms g^{-1}).

5.2. ^{26}Al/^{10}Be Ratios

The error-weighted mean of ^{26}Al/^{10}Be ratios for deglacial sand (correcting for Holocene nuclide production) and modern sediment samples (6.1±0.3 and 6.6±0.5, respectively, one standard deviation) are lower than the measured Greenland production ratio of 7.3±0.3 but more similar to that at mid-latitudes of ~6.8 (Figure 5C, p = 0.01, Corbett et al., 2017). The ^{26}Al/^{10}Be ratios for deglacial samples are more variable (IQR = 2.24) than ratios measured in modern stream samples (IQR = 0.78, Figure 5C).

The ^{26}Al/^{10}Be of deglacial samples exhibit a significant, positive linear trend with increasing distance from the middle of the QLID (r^2 = 0.45, p = 0.03) (Figure 6). The five samples closest to the middle of the ice dome (5.3±0.4) have lower error-weighted average ^{26}Al/^{10}Be ratios than five samples farther away (7.0±0.4, Figure 6). Modern samples, in contrast, exhibit no spatial trend in ^{26}Al/^{10}Be ratios. Tukey HSD tests show a significant difference between ^{26}Al/^{10}Be ratios in deglacial samples closest to and further from the middle of the ice dome (both tests: $p < 0.01$).

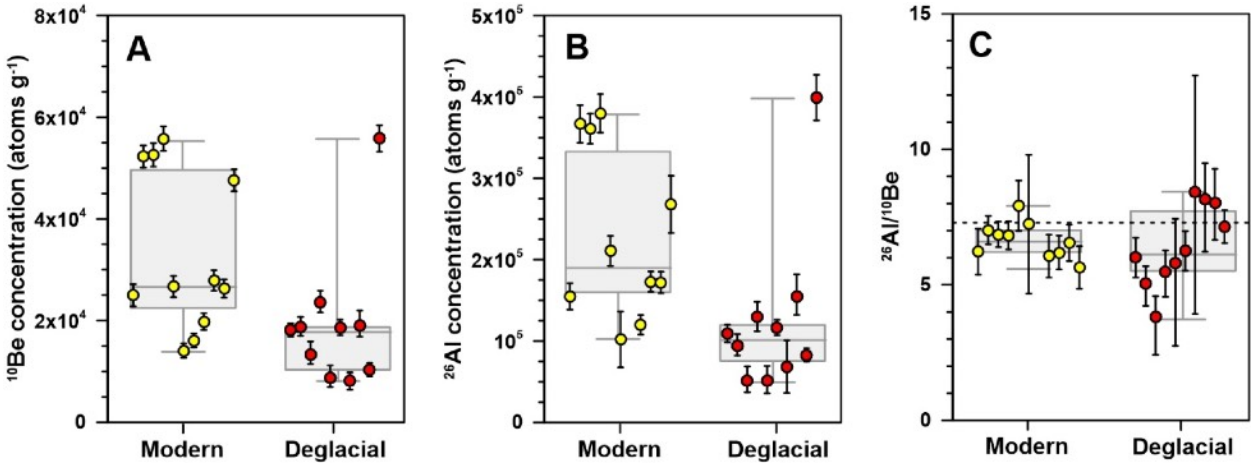

Figure 5. Comparison of modern and Holocene-exposure-corrected deglacial samples. (A) ^{10}Be concentrations, (B) ^{26}Al concentrations, and (C) ^{26}Al/^{10}Be ratios for deglacial (Holocene-corrected) and modern samples. The dashed line in panel C indicates the empirical production ratio (7.3) at high latitudes from Corbett et al. (2017). Points represent individual samples with 1σ propagated errors for modern (yellow) and deglacial (red) samples. Box and

whisker plots are shown for each dataset with whiskers going to the smallest and highest values. The box extends from the 25th to the 75th percentiles. The line in the middle of each box is the median.

Table 4. Holocene Exposure-Corrected Isotopic Data for Deglacial Samples

Sample Name	Distance from Labrador City	Inherited ^{10}Be (atoms g^{-1})	^{10}Be Uncertainty (atoms g^{-1}) [a]	Inherited ^{26}Al (atoms g^{-1})	^{26}Al Uncertainty (atoms g^{-1}) [a]	Inherited ^{26}Al/^{10}Be	^{26}Al/^{10}Be Uncertainty [a]
CF-02	221	1.82 x 10^4	(-1.03, +1.03) x 10^3	1.09 x 10^5	(-1.08, +1.08) x 10^4	6.00	-0.74, +0.76
LC-02	109	1.87 x 10^4	(-2.03, +1.69) x 10^3	9.43 x 10^4	(-1.44, +1.422 x 10^4	5.05	-0.82, +0.65
LC-04	162	1.33 x 10^4	(-2.57, +1.88) x 10^3	5.09 x 10^4	(-1.80, +1.36) x 10^4	3.81	-1.40, +0.77
LC-05	188	2.36 x 10^4	(-2.27, +2.03) x 10^3	1.30 x 10^5	(-1.88, +1.75) x 10^4	5.49	-0.93, +0.78
MC-01	309	8.81 x 10^3	(-2.33, +1.83) x 10^3	5.11 x 10^4	(-1.82, +1.54) x 10^4	5.80	-3.06, +1.64
MC-02	506	1.86 x 10^4	(-1.54, +1.54) x 10^3	1.17 x 10^5	(-9.56, +9.56) x 10^3	6.25	-0.73, +0.73
GB-03	403	8.12 x 10^3	(-1.69, +1.68) x 10^3	6.84 x 10^4	(-3.23, +3.23) x 10^4	8.42	-4.49, +4.30
GB-05	361	1.90 x 10^4	(-2.97, +2.15) x 10^3	1.55 x 10^5	(-2.68, +2.29) x 10^4	8.15	-1.93, +1.33
SS-01	580	1.03 x 10^4	(-1.34, +1.29) x 10^3	8.29 x 10^4	(-8.40, +7.99) x 10^3	8.02	-1.37, +1.25
SS-05	710	5.59 x 10^4	(-2.63, +2.63) x 10^3	3.99 x 10^5	(-2.81, +2.81) x 10^4	7.15	-0.61, +0.61
GB-06	285	1.79 x 10^4	3.90 x 10^3	2.15 x 10^5	2.90 x 10^4	12.0	3.07

[a]Uncertainties account for both analytical and sample depth uncertainties. The depth uncertainties in combination with nonlinear production rate changes with depth yield asymmetrical nuclide uncertainties. Uncertainties are 1σ.

Figure 6. ^{26}Al/^{10}Be ratios versus distance from middle of the QLID which we have designated as Labrador City. Deglacial data are corrected for Holocene nuclide production and fit with a trendline. Error bars are 1σ. Dashed line shows production ratio at high latitudes (7.3, Corbett et al., 2017).

6. Discussion

Measurements of in situ-produced ^{10}Be and ^{26}Al, presented here and in previously published papers, indicate that many samples of bedrock (57%), erratic boulders (34%), and deglacial sediment (100%), collected from terrain once covered by the QLID of the LIS, contain cosmogenic nuclides accumulated during periods of exposure prior to the last deglaciation. Our findings for bedrock and boulders are remarkably similar to those of a compilation of nearly 1000 samples collected from areas overrun by the Fennoscandian Ice Sheet and analyzed for cosmogenic nuclides (Jansen et al., 2019). Those authors found that 27% of erratic boulders contain inherited nuclides along with 64% of sampled bedrock outcrops (Jansen et al., 2019).

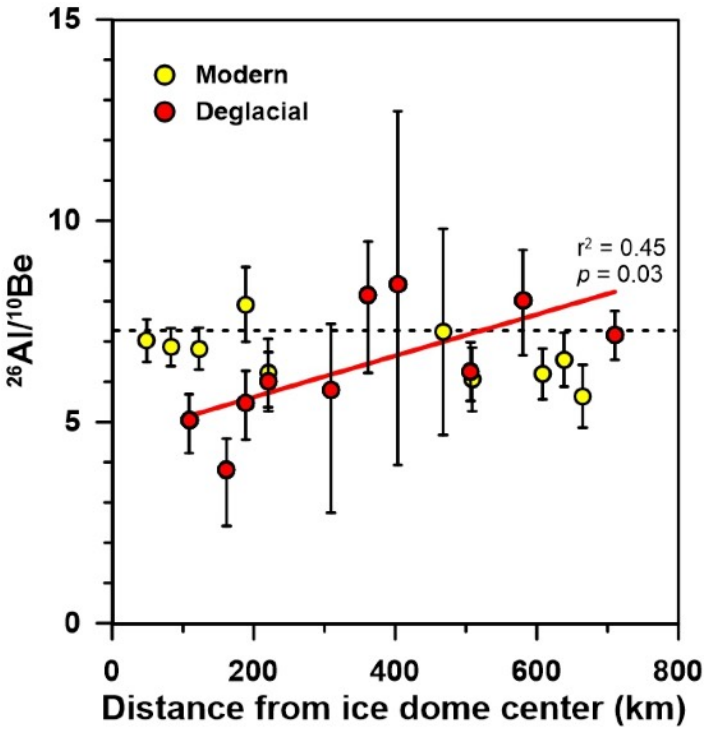

These data, along with many other data sets, show convincingly that in areas once covered by temperate, mid-latitude ice sheets, nuclide inheritance from periods of prior exposure is geographically widespread, commonplace, and spatially variable in both detrital and bedrock samples. Our analysis of glacial sediment presented in this paper provides a different way of examining the magnitude of inheritance because it averages nuclide concentrations retained in earth materials from periods of exposure prior to the LGM on a landscape-scale. Such averaging avoids potential spatial bias of point measurements on outcrops and erratic boulders and provides a more generalized view of glacial erosion, sediment residence and transport times, and cosmogenic nuclide inheritance.

6.1 Differences in ^{10}Be inheritance between sample types

Compilation of extant cosmogenic data shows that samples collected from erratic boulders contain lower average concentrations of inherited ^{10}Be (14,000 atoms g^{-1}) than those collected from bedrock outcrops (120,700 atoms g^{-1}) and deglacial sediment (19,500 atoms g^{-1}, Figures 7 and 8). Of the 192 reported boulder analyses, we calculate that 65 boulder samples (34% of total) contain ^{10}Be inherited from pre-LGM periods of exposure on the basis of having >3000 atoms g^{-1} of ^{10}Be (the median analytical uncertainty) above that produced during deglacial exposure as determined from Dalton et al.'s (2020) isochrons. The average boulder inheritance is equal to ~1800 years of surface exposure, a value skewed high by relatively few boulders with large concentrations of inherited nuclides. In contrast, the median boulder age is about 650 years younger than Dalton et al.'s (2020) radiocarbon-based chronology. Such a discrepancy between median boulder exposure ages and radiocarbon ages of organic material likely reflects a combination of boulder surface erosion, boulder burial by snow or till (Schildgen et al.,

2005), ^{10}Be production rate uncertainty (Balco et al., 2009), the effect of isostatic uplift on nuclide production rates, and the incorporation of old carbon in radiocarbon dated samples (see references in Halsted et al., 2024).

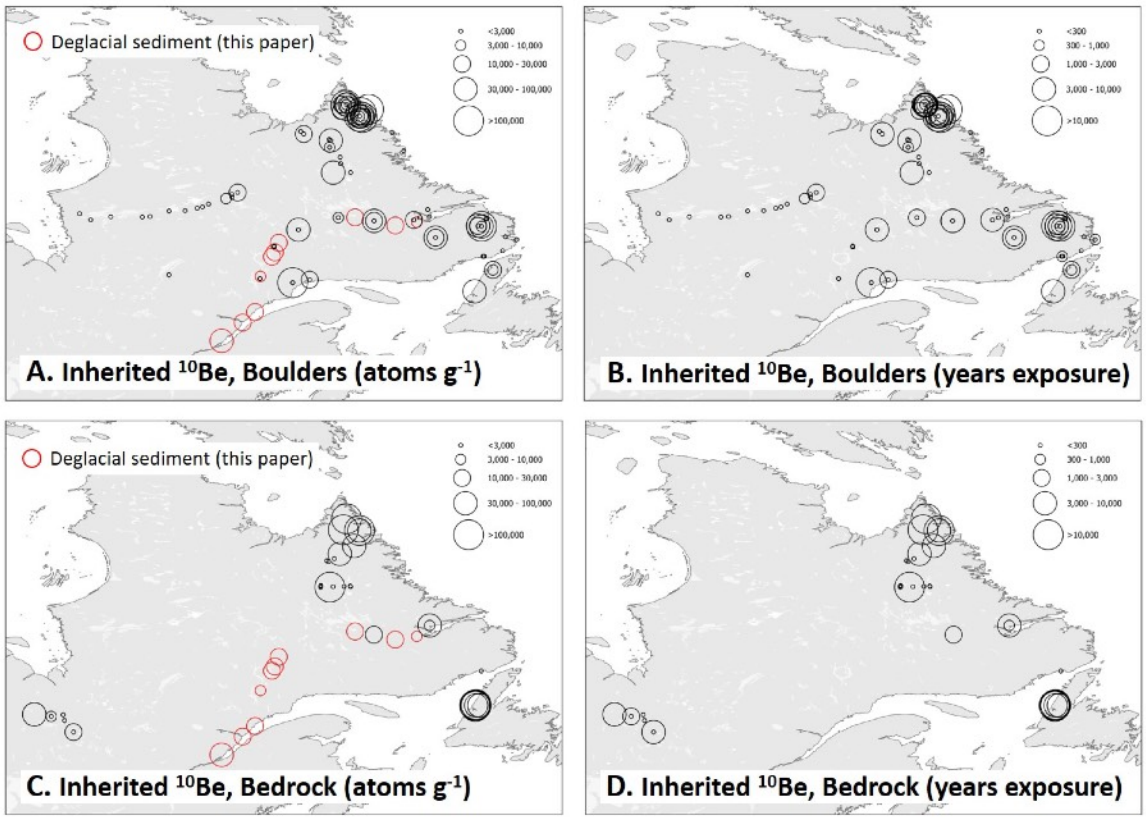

,

Figure 7. Spatial distribution of inheritance interpreted from published data corrected using deglacial age model of Dalton et al. (2020). A. Boulder data, atoms g^{-1} inherited ^{10}Be. B. Boulder data, inherited years equivalent surface exposure. C. Bedrock data, atoms g^{-1} inherited ^{10}Be. B. Bedrock data, inherited years equivalent surface exposure. Red circles are deglacial sediment data (this paper). Inheritance scaled to circle diameter.

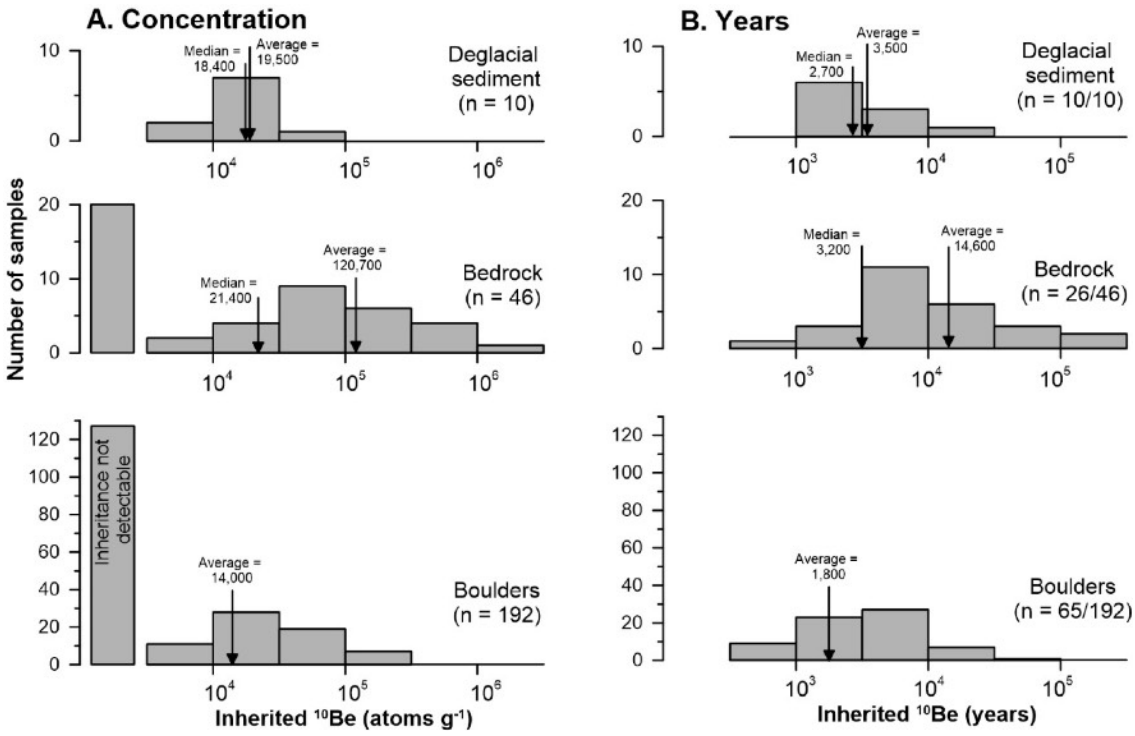

Figure 8. Histograms (logarithmic) of inherited ^{10}Be in deglacial sediment (this study), glaciated bedrock (this study and others), and erratic boulders (other studies) sampled from eastern Canadian landscapes once covered by the QLID of the LIS. A. Inheritance (atoms g^{-1}). B. Inheritance expressed as years of surface exposure calculated using site-specific ^{10}Be production rates to remove elevation dependence of nuclide production rates. Sample count, average, and median values indicated with arrows. Values < 3000 atoms g^{-1}, the median uncertainty in measurements, are considered to have no detectable inheritance and are counted as zero for statistical analysis.

We find that 26 of 46 sampled bedrock outcrops (57%) contain detectable ^{10}Be (mean =120,700 atoms g^{-1}; median = 21,400 atoms g^{-1}) inherited from pre-LGM periods of exposure. Considered as exposure time, this is an average inheritance for bedrock samples of 14,600 years. Because the distribution is skewed, the median inheritance, when considered as a surface exposure time, is less—3200 years (Figure 7). Lower mean and median concentrations of inherited nuclides in erratic boulders than in exposed bedrock from beneath the former QLID suggest that the boulders were quarried from below the present-day bedrock surface, are preferentially derived from more erosive areas of the ice sheet, and/or were reworked from deposits deep enough that interglacial exposure to cosmic radiation was insufficient to create high concentrations of ^{10}Be.

All 10 deglacial sand samples (100%) contain inherited nuclides (median =18,400 atoms g^{-1}; mean = 19,500 atoms g^{-1}), the equivalent of 2700 and 3500 years of surface exposure (Figure 7). Unlike the distribution of boulder and bedrock sample ^{10}Be concentrations, that of deglacial sand samples is not skewed as indicated by the similarity of the mean and median. This similarity likely reflects the physical mixing of thousands of sand grains included in the sediment samples, each with its own idiosyncratic burial and exposure history. We recognize that

there is likely a sampling bias in the location of bedrock and boulder samples – at least in part dictated by limited road access. Sediment samples, because they integrate across much larger areas, are likely less subject to such a bias.

We conducted a sensitivity analysis, which shows that our finding of nuclide inheritance is robust to uncertainty in the time/retreat distance model that we used to correct for post-depositional nuclide production. For surface boulder and bedrock samples, if Dalton et al.'s (2020) retreat chronology were 10% too old, then the number of such samples with inheritance above analytical uncertainty (3,000 atoms g^{-1}) would increase from 90 to 120. Conversely, if the Dalton et al. (2020) model reported deglacial ages that were 10% too young, then the number of samples with inheritance would decrease from 90 to 75. For buried deglacial sand samples, the influence of the age model is much less than for boulders and bedrock collected at the surface because the cosmic-flux is strongly attenuated with depth.

Because isostatic uplift in response to deglaciation has raised sample sites to higher elevations than they were at the time of deglaciation, nuclide production rates at the sampling locations have increased over time (Jones et al., 2019). Using the uplift-corrected data provided in Dalton et al. (2023), we calculated that accounting for such post-glacial uplift would increase the concentration of nuclides inherited at initial exposure by 3400±2400 atoms g^{-1}. While such a correction is uncertain, it suggests that our estimates of nuclides inherited from periods of prior exposure are likely conservative.

6.2 Spatial variability in ice sheet erosion depth

Our compilation of data from 248 samples (deglacial sediment and surface bedrock samples, this paper, and prior published bedrock and boulder data, supplemental information) analyzed for cosmogenic nuclides indicates that the QLID of the LIS did not deeply or uniformly erode its bed, nor did it effectively remove cosmogenic nuclides produced in sediment and rock exposed during prior interglacial periods (Figures 7 and 8). The broad distribution of inherited ^{10}Be in bedrock is consistent with spatially variable ice sheet erosivity and/or varying thickness of interglacial sediment cover shielding the underlying rock from cosmic rays when the ice was gone and has been noted by others, particularly at high elevations in the eastern part of the study area (Marquette et al., 2004; Staiger et al., 2005).

Subglacial process modeling over eastern North America (Melanson et al., 2013) suggests a variably erosive LIS in Quebec and Labrador during the last glacial cycle consistent with our findings. Melanson et al. (2013) suggest that total erosion per glacial cycle, predicted using empirical abrasion and quarrying laws, ranges from near zero under the middle of the Quebec-Labrador dome to ≥10 m along parts of its Atlantic and St. Lawrence margin. Melanson et al.'s (2013) numerical modeling of the Quebec-Labrador region exhibits similar minima for both basal sliding speed and total ice movement integrated over the last glacial cycle – both variables related to the efficacy of glacial erosion. Simulated ice sliding distances (the integrated basal velocity over the last glacial cycle in millions of meters, Mm) are near zero in the middle of our study area, 1 Mm near Goose Bay, and 3 Mm along the St. Lawrence estuary – an order of magnitude less than for the Hudson Strait ice stream and southern LIS lobes (Melanson et al., 2013). Landscape analysis using remotely sensed data also suggests variable bed conditions and erosion efficacy of the LIS QLID over time and space (Rice et al., 2020).

The average inherited nuclide concentration we measured in LIS deglacial sediment (19,500 ^{10}Be atoms g^{-1}) is several times higher than the average found in sediment shed by the Greenland Ice Sheet today (~6,500 ^{10}Be atoms g^{-1}, Nelson et al., 2014) but much lower than those deposited by the LIS in the midwestern United States (~60,000 ^{10}Be atoms g^{-1}, Balco, 2005). The low concentrations of ^{10}Be in sediment issuing from the Greenland Ice Sheet (as well as low ^{26}Al/^{10}Be ratios ~4.5, Bierman et al., 2016) reflect continuous ice cover through many Pleistocene interglacials and erosive warm-based ice in areas from which sediment is sourced. In contrast, the high concentrations of ^{10}Be in deglacial sediment originating from the southern margin of the Keewatin Ice Dome in Minnesota (Balco, 2005) suggest that ice there was frequently absent and when present, only weakly erosive. Some data suggest that in central North America the LIS was at least in part, cold-based near the margin (c.f., Colgan et al., 2002).

6.3 Implications for sample collection and surface exposure dating

Both our compilation (LIS) and that for the Fennoscandian Ice Sheet of Jansen et al. (2019) differ from that of Heyman et al. (2011) who, 15 years prior to our work, suggested that "few boulders from the paleo-ice sheets have exposure ages significantly older than independently known deglaciation ages, indicating that prior exposure is of limited significance." This difference likely reflects numerous additional cosmogenic nuclide measurements that have been made since the publication of Heyman et al. (2011), a time over which AMS measurement precision has greatly improved and the number of other pertinent dates using different chronometers to constrain the time of deglaciation has increased. As Heyman et al. (2011) clearly point out, such inheritance, if not detected and corrected for, has the potential to increase cosmogenic exposure ages, biasing them high, including those from exposed rock and glacial deposits.

The new and compiled data have implications for sample collection and interpretation in areas once covered by now-vanished ice sheets, specifically the QLID of the LIS. The compiled data show clearly that sampling boulders rather than bedrock is most likely to minimize the influence on calculated landform age of nuclides inherited from exposure prior to the last deglaciation. Because the distributions of inherited ^{10}Be concentrations in both the bedrock and boulder populations are skewed (Figure 7), extreme outliers are potentially detectable. Indeed, Ullman et al. (2016) excluded 10 of 65 boulder samples because of their unusually high concentration of ^{10}Be. Couette et al., (2023) similarly excluded 5 of 37 samples in eastern Labrador because of high ^{10}Be concentrations.

Lower concentrations of inherited nuclides, likely the result of deeply penetrating muons during interglacial times without ice cover, are more difficult to detect and correct for. This inheritance could skew slightly the average age of an exposure age data set. In that regard, the depth profile data (samples LBD19-46-52) are illustrative because they are consistent with several thousand atoms g^{-1} of inherited nuclides at depth of several meters (Figure 4). Such inheritance would increase exposure ages of plucked boulders and glacially eroded outcrops by hundreds of years (a phenomenon noted by Ullman et al. (2016) who reported that ^{10}Be-based deglacial chronology was older than radiocarbon-based estimates of local deglaciation by centuries, their Figure 7).

hile radiocarbon age lags have been attributed to delayed colonization of the landscape by vegetation following deglaciation (e.g., Halsted et al., 2024; Peteet et al., 2012), the nuclide inheritance we find in Quebec and

Labrador suggests that in this region, many ^{10}Be ages from boulder and bedrock samples will be too old by at least hundreds of years. The overall agreement of the Ullman et al. (2016) cosmogenic ages with those of Dalton et al. (2022) and Dyke (2004) suggests that in our study area a population of boulder dates, screened for outliers, is likely to be representative of deglaciation age at ky resolution.

6.4 Interglacial presence of QLID and ^{26}Al/^{10}Be ratio of IRD

Finding ^{26}Al/^{10}Be ratios below the nominal Arctic surface production ratio of 7.3 (Corbett et al., 2017) in quartz IRD from North Atlantic Heinrich layers, LeBlanc et al. (2023) suggested that ice sheet remnants may have lingered in parts of eastern Canada for the majority of Pleistocene interglacials burying the land surface and allowing for the ^{26}Al/^{10}Be ratio to lower by radioactive decay (Figure 9). While Heinrich layer sediment was predominantly delivered to the ocean by the Hudson Strait ice stream (Bond et al., 1992), the quartz IRD that LeBlanc et al. (2023) analyzed most likely came from interior areas of the LIS (where crystalline rocks crop out) as opposed to Hudson Strait, which is primarily underlain by carbonate rocks. Burial by till or in outwash deposits could have the same effect – but with the paucity of glacial sediment over most of the QLID landscape (Pelletier et al., 2016), burial of a sufficient volume of sediment at depths of many meters seems implausible.

Depressed ^{26}Al/^{10}Be ratios in the Holocene exposure-corrected deglacial sediment that we sampled are consistent with ice lingering near Labrador City (the middle of the ice dome) for at least some interglacial periods, shielding rock and sediment below from cosmic rays (Figure 6). In contrast, the higher ^{26}Al/^{10}Be ratios in deglacial sediment toward the edge of the ice dome are consistent with repeated exposure during interglacials. Thus, it appears that the quartz analyzed by LeBlanc et al. (2023) is unlikely to have been sourced from much of the area we sampled in southeastern Canada.

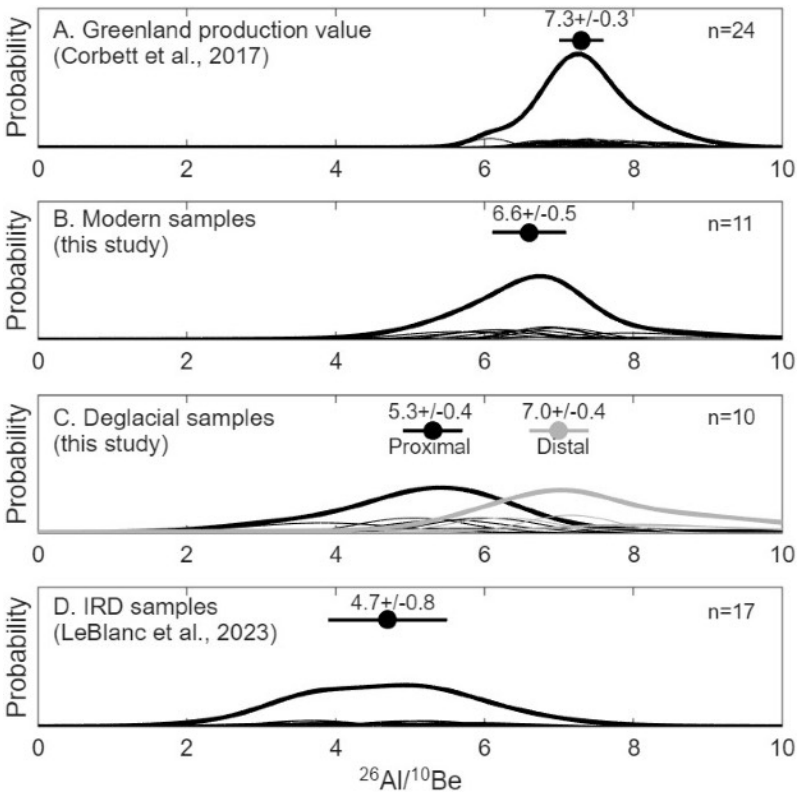

Figure 9. Summed probability plots of $^{26}Al/^{10}Be$ ratios for Arctic samples. A. Samples with simple exposure histories in Greenland (Corbett et al., 2017). B. Modern stream sediment (this study). C. Deglacial samples corrected for Holocene exposure; black 5 samples most proximal to Labrador City (approximate middle of the dome); grey 5 samples are most distal (this study). D. IRD samples from North Atlantic (LeBlanc et al., 2023). Analytical error-weighted mean and 1 SD uncertainty above each plot.

It is possible that incorporation of the IRD sampled by LeBlanc et al. (2023) occurred primarily toward the middle of the QLID and not closer to the margins. It is also possible that the IRD sampled by LeBlanc et al. (2023) was sourced from a wider area (the Keewatin Dome and/or Baffin Island) where samples of sediment (Balco, 2005) and those taken from outcrops (Corbett et al., 2016c; Marsella et al., 2000) have sufficiently low $^{26}Al/^{10}Be$ ratios to match those measured by LeBlanc et al. (2023). Low ratios would also result if IRD were stored in Hudson Bay for ~1 Ma before transport to the deep sea, during which time ^{26}Al and ^{10}Be would decay and the $^{26}Al/^{10}Be$ ratio would decrease. More extensive sampling of eastern Canada, including Quebec-Labrador, and farther north near Hudson Bay and Baffin Island, would provide further evidence on how persistent different sectors of the eastern LIS were during Pleistocene interglacials.

6.5 Sediment Sourcing in Modern Rivers

We estimate the percentage of sediment derived from erosion of deglacial materials using a two-component, linear-mixing model based on the measured average concentrations of ^{10}Be in both river and deglacial

sediment and assumptions about nuclide production since deglaciation. One component is deglacial deposits which, based on our sampling, contain an average of 22.5 x 10^3 ^{10}Be atoms g^{-1} and enter rivers by bank incision (Figure 2A). The second component is surficial materials which, when eroded, enter the drainage network.

Since we did not sample these surficial materials directly, we calculate their ^{10}Be concentration by assuming that, at the time of deglaciation (the beginning of exposure), surface sediment contained the average Holocene exposure-corrected concentration of ^{10}Be for deglacial sediment (19.5 x 10^3 ^{10}Be atoms g^{-1}). We then use the average deglacial age of 9.32 ka for our field area and the average ^{10}Be surface production rate (7.82 atoms y^{-1} g^{-1}) to calculate that surface material gained about 7.3 x 10^4 ^{10}Be atoms g^{-1} since deglaciation. The surface-exposed end member therefore contains 92.3 x 10^3 ^{10}Be atoms g^{-1}.

Knowing that modern sediment contains on average 33.1 x 10^3 ^{10}Be atoms g^{-1} (Table 3), the two-component mixing model suggests that about 85% of sediment in eastern Quebec and Labrador rivers today is derived from incision of glacial deposits and the remaining about 15% comes from erosion of surficial sediment and bedrock. Our findings for eastern Quebec and Labrador are similar to those of Balco (2005) in Minnesota. In that previously glaciated region, they suggest most sediment carried by contemporary rivers comes from incision of glacial deposits. Our finding is also consistent with the low sediment yield of forested upland terrains in other glaciated areas of the LIS (e.g., Dethier et al., 2018).

7.0 Conclusions

Analysis of cosmogenic ^{10}Be and ^{26}Al in deglacial (n=10) sediment samples, in a bedrock depth profile (n=7), in our new as well as previously-published boulders and bedrock sample data (n=238), and in one bedrock sample we collected, indicates that nuclides produced during prior interglacial exposures are commonplace in samples collected from the landscape beneath the now-vanished QLID of the LIS. These isotopic data indicate erosion depths in bedrock are no more than a few meters per glacial cycle and/or that regolith generated and exposed during previous glacial and interglacial cycles was not efficiently removed from the terrestrial landscape during the last glaciation. Such inheritance explains numerous outliers in previously published data sets and suggests pervasive inheritance of low concentrations of in situ produced cosmogenic nuclides. Boulders in the area covered by the QLID appear to carry, on average, lower concentrations of inherited nuclides than bedrock outcrops suggesting that dating studies with limited resources may benefit from sampling boulders rather than bedrock. On average, nuclide concentrations in modern fluvial sediment are only slightly higher than those in deglacial sediment, implying most sand, transported by rivers today in landscapes once covered by the QLID, is sourced from eroding banks composed of glacial deposits rather than surrounding land surfaces.

Author contribution

Bierman and Shakun conceived and designed the study. Cavnar, LeBlanc, and Shakun collected samples. Cavnar performed sample preparation under the supervision of Corbett. Caffee assisted with statistical analysis and oversaw measurement of cosmogenic nuclides via AMS at PRIME Lab. Couette and Ghienne collected the bedrock depth profile samples. Couette performed sample preparation and data analysis under the supervision of Van der Woerd. Cavnar drafted the initial manuscript and performed initial data reduction and statistical analysis. Shakun and

Bierman performed data compilation and inheritance analysis. All authors assisted with conceptual design of figures, manuscript organization, and editing. Bierman and Shakun revised the manuscript after two cycles of peer review.

Competing Interests

The authors declare that they have no conflict of interest.

Acknowledgements

We thank the 2022 field sampling team including Juliana Souza, Halley Mastro, and Cat Collins. Funding for this research was provided by NSF-EAR-2300560, 2116209, 2114629, and 1735676 awards to Bierman and Corbett, 2116208 to Shakun, NSF-OPP-PRF 2420274 post-doctoral fellowship to LeBlanc, NSERC grants to Lajeunesse, and institutional grants to Ghienne. The French national AMS facility ASTER (CEREGE) is supported by the INSU/CNRS, the French MESR, and the CEA institute. We thank G. Aumaître and K. Keddadouche for the AMS measurements at ASTER.

References Cited

Alley, R. B., Cuffey, K. M., and Zoet, L. K.: Glacial erosion: status and outlook, Annals of Glaciology, 60, 1–13, https://doi.org/10.1017/aog.2019.38, 2019.

Amani, M., Mahdavi, S., Afshar, M., Brisco, B., Huang, W., Mohammad Javad Mirzadeh, S., White, L., Banks, S., Montgomery, J., and Hopkinson, C.: Canadian wetland inventory using Google Earth Engine: the first map and preliminary results, Remote Sensing, 11, 842, https://doi.org/10.3390/rs11070842, 2019.

Andrews, J. T. and Tyler, K.: The observed postglacial recovery of Québec and Nouveau-Québec Since 12,000 BP, Géographie physique et Quaternaire, 31, 389–400, https://doi.org/10.7202/1000286ar, 2011.

Balco, G.: Dating Plio-Pleistocene glacial sediments using the cosmic-ray-produced radionuclides ^{10}Be and ^{26}Al, American Journal of Science, 305, 1–41, https://doi.org/10.2475/ajs.305.1.1, 2005.

Balco, G. and Rovey, C. W.: An isochron method for cosmogenic-nuclide dating of buried soils and sediments, American Journal of Science, 308, 1083–1114, https://doi.org/10.2475/10.2008.02, 2008.

Balco, G. and Rovey, C. W.: Absolute chronology for major Pleistocene advances of the Laurentide Ice Sheet, Geology, 38, 795–798, https://doi.org/10.1130/G30946.1, 2010.

Balco, G., Stone, J. O. H., Porter, S. C., and Caffee, M. W.: Cosmogenic-nuclide ages for New England coastal moraines, Martha's Vineyard and Cape Cod, Massachusetts, USA, Quaternary Science Reviews, 21, 2127–2135, https://doi.org/10.1016/S0277-3791(02)00085-9, 2002.

Balco, G., Stone, J. O., Lifton, N. A., and Dunai, T. J.: A complete and easily accessible means of calculating surface exposure ages or erosion rates from ^{10}Be and ^{26}Al measurements, Quaternary Geochronology, 3, 174–195, https://doi.org/10.1016/j.quageo.2007.12.001, 2008.

Balco, G., Briner, J., Finkel, R. C., Rayburn, J. A., Ridge, J. C., and Schaefer, J. M.: Regional beryllium-10 production rate calibration for late-glacial northeastern North America, Quaternary Geochronology, 4, 93–107, https://doi.org/10.1016/j.quageo.2008.09.001, 2009.

Balter-Kennedy, A., Schaefer, J. M., Balco, G., Kelly, M. A., Kaplan, M. R., Schwartz, R., Oakley, B., Young, N. E., Hanley, J., and Varuolo-Clarke, A. M.: The Laurentide Ice Sheet in southern New England and New York during and at the end of the Last Glacial Maximum: a cosmogenic-nuclide chronology, Clim. Past, 20, 2167–2190, https://doi.org/10.5194/cp-20-2167-2024, 2024.

Barth, A. M., Marcott, S. A., Licciardi, J. M., and Shakun, J. D.: Deglacial Thinning of the Laurentide Ice Sheet in the Adirondack Mountains, New York, USA, Revealed by^{36} Cl Exposure Dating, Paleoceanog and Paleoclimatol, 34, 946–953, https://doi.org/10.1029/2018PA003477, 2019.

Batchelor, C. L., Margold, M., Krapp, M., Murton, D. K., Dalton, A. S., Gibbard, P. L., Stokes, C. R., Murton, J. B., and Manica, A.: The configuration of Northern Hemisphere ice sheets through the Quaternary, Nat Commun, 10, 3713, https://doi.org/10.1038/s41467-019-11601-2, 2019.

Beck, H. E., Zimmermann, N. E., McVicar, T. R., Vergopolan, N., Berg, A., and Wood, E. F.: Present and future Köppen-Geiger climate classification maps at 1-km resolution, Sci Data, 5, 180214, https://doi.org/10.1038/sdata.2018.214, 2018.

Bierman, P. R., Marsella, K. A., Patterson, C., Davis, P. T., and Caffee, M.: Mid-Pleistocene cosmogenic minimum-age limits for pre-Wisconsinan glacial surfaces in southwestern Minnesota and southern Baffin Island: a multiple nuclide approach, Geomorphology, 27, 25–39, https://doi.org/10.1016/S0169-555X(98)00088-9, 1999.

Bierman, P. R., Marsella, K. A., Davis, P. T., and Caffee, M. W.: Response to Discussion by Wolfe et al. on Bierman et al. (Geomorphology 25 (1999) 25–39), Geomorphology, 39, 255–260, https://doi.org/10.1016/S0169-555X(00)00102-1, 2001.

Bierman, P. R., Caffee, M. W., Davis, P. T., Marsella, K., Pavich, M., Colgan, P., Mickelson, D., and Larsen, J.: Rates and Timing of Earth Surface Processes From In Situ-Produced Cosmogenic Be-10, Reviews in Mineralogy and Geochemistry, 50, 147–205, https://doi.org/10.2138/rmg.2002.50.4, 2002.

Bierman, P. R., Davis, P. T., Corbett, L. B., Lifton, N. A., and Finkel, R. C.: Cold-based Laurentide ice covered New England's highest summits during the Last Glacial Maximum, Geology, G37225.1, https://doi.org/10.1130/G37225.1, 2015.

Bierman, P. R., Shakun, J. D., Corbett, L. B., Zimmerman, S. R., and Rood, D. H.: A persistent and dynamic East Greenland Ice Sheet over the past 7.5 million years, Nature, 540, 256–260, https://doi.org/10.1038/nature20147, 2016.

Bierman, P. R., Mastro, H. M., Peteet, D. M., Corbett, L. B., Steig, E. J., Halsted, C. T., Caffee, M. M., Hidy, A. J., Balco, G., Bennike, O., and Rock, B.: Plant, insect, and fungi fossils under the center of Greenland's ice sheet are evidence of ice-free times, Proc. Natl. Acad. Sci. U.S.A., 121, e2407465121, https://doi.org/10.1073/pnas.2407465121, 2024a.

Bierman, P. R., Christ, A. J., Collins, C. M., Mastro, H. M., Souza, J., Blard, P.-H., Brachfeld, S., Courville, Z. R., Rittenour, T. M., Thomas, E. K., Tison, J.-L., and Fripiat, F.: Scientific history, sampling approach, and physical characterization of the Camp Century subglacial material, a rare archive from

beneath the Greenland Ice Sheet, The Cryosphere, 18, 4029–4052, https://doi.org/10.5194/tc-18-4029-2024, 2024b.

Blard, P.-H., Protin, M., Tison, J.-L., Fripiat, F., Dahl-Jensen, D., Steffensen, J. P., Mahaney, W. C., Bierman, P. R., Christ, A. J., Corbett, L. B., Debaille, V., Rigaudier, T., Claeys, P., and ASTER Team: Basal debris of the NEEM ice core, Greenland: a window into sub-ice-sheet geology, basal ice processes and ice-sheet oscillations, J. Glaciol., 69, 1011–1029, https://doi.org/10.1017/jog.2022.122, 2023.

Bond, G., Heinrich, H., Broecker, W., Labeyrie, L., McManus, J., Andrews, J., Huon, S., Jantschik, R., Clasen, S., Simet, C., Tedesco, K., Klas, M., Bonani, G., and Ivy, S.: Evidence for massive discharges of icebergs into the North Atlantic ocean during the last glacial period, Nature, 360, 245–249, https://doi.org/10.1038/360245a0, 1992.

Booth, D. B.: Glaciofluvial infilling and scour of the Puget Lowland, Washington, during ice-sheet glaciation, Geol, 22, 695, https://doi.org/10.1130/0091-7613(1994)022%253C0695:GIASOT%253E2.3.CO;2, 1994.

Braucher, R., Bourlès, D., Merchel, S., Vidal Romani, J., Fernadez-Mosquera, D., Marti, K., Léanni, L., Chauvet, F., Arnold, M., Aumaître, G., and Keddadouche, K.: Determination of muon attenuation lengths in depth profiles from in situ produced cosmogenic nuclides, Nuclear Instruments and Methods in Physics Research Section B: Beam Interactions with Materials and Atoms, 294, 484–490, https://doi.org/10.1016/j.nimb.2012.05.023, 2013.

Braucher, R., Guillou, V., Bourlès, D. L., Arnold, M., Aumaître, G., Keddadouche, K., and Nottoli, E.: Preparation of ASTER in-house 10Be/9Be standard solutions, Nuclear Instruments and Methods in Physics Research Section B: Beam Interactions with Materials and Atoms, 361, 335–340, https://doi.org/10.1016/j.nimb.2015.06.012, 2015.

Briner, J. P. and Swanson, T. W.: Using inherited cosmogenic 36Cl to constrain glacial erosion rates of the Cordilleran ice sheet, Geol, 26, 3, https://doi.org/10.1130/0091-7613(1998)026%253C0003:UICCTC%253E2.3.CO;2, 1998.

Briner, J. P., Miller, G. H., Davis, P. T., and Finkel, R. C.: Cosmogenic radionuclides from fiord landscapes support differential erosion by overriding ice sheets, Geological Society of America Bulletin, 118, 406–420, https://doi.org/10.1130/B25716.1, 2006.

Briner, J. P., Goehring, B. M., Mangerud, J., and Svendsen, J. I.: The deep accumulation of ^{10}Be at Utsira, southwestern Norway: Implications for cosmogenic nuclide exposure dating in peripheral ice sheet landscapes, Geophysical Research Letters, 43, 9121–9129, https://doi.org/10.1002/2016GL070100, 2016.

Carlson, A. E., Clark, P. U., Raisbeck, G. M., and Brook, E. J.: Rapid Holocene Deglaciation of the Labrador Sector of the Laurentide Ice Sheet, Journal of Climate, 20, 5126–5133, https://doi.org/10.1175/JCLI4273.1, 2007.

Christ, A. J., Bierman, P. R., Knutz, P. C., Corbett, L. B., Fosdick, J. C., Thomas, E. K., Cowling, O. C., Hidy, A. J., and Caffee, M. W.: The Northwestern Greenland Ice Sheet during the Early Pleistocene was similar to today, Geophysical Research Letters, 47, https://doi.org/10.1029/2019GL085176, 2020.

Christ, A. J., Bierman, P. R., Schaefer, J. M., Dahl-Jensen, D., Steffensen, J. P., Corbett, L. B., Peteet, D. M., Thomas, E. K., Steig, E. J., Rittenour, T. M., Tison, J.-L., Blard, P.-H., Perdrial, N., Dethier, D. P., Lini, A., Hidy, A. J., Caffee, M. W., and Southon, J.: A multimillion-year-old record of Greenland

vegetation and glacial history preserved in sediment beneath 1.4 km of ice at Camp Century, Proc. Natl. Acad. Sci. U.S.A., 118, e2021442118, https://doi.org/10.1073/pnas.2021442118, 2021.

Christ, A. J., Rittenour, T. M., Bierman, P. R., Keisling, B. A., Knutz, P. C., Thomsen, T. B., Keulen, N., Fosdick, J. C., Hemming, S. R., Tison, J.-L., Blard, P.-H., Steffensen, J. P., Caffee, M. W., Corbett, L. B., Dahl-Jensen, D., Dethier, D. P., Hidy, A. J., Perdrial, N., Peteet, D. M., Steig, E. J., and Thomas, E. K.: Deglaciation of northwestern Greenland during Marine Isotope Stage 11, Science, 381, 330–335, https://doi.org/10.1126/science.ade4248, 2023.

Clark, P. U., Brook, E. J., Raisbeck, G. M., Yiou, F., and Clark, J.: Cosmogenic 10Be ages of the Saglek Moraines, Torngat Mountains, Labrador, Geol, 31, 617, https://doi.org/10.1130/0091-7613(2003)031%253C0617:CBAOTS%253E2.0.CO;2, 2003.

Colgan, P. M., Bierman, P. R., Mickelson, D. M., and Caffee, M.: Variation in glacial erosion near the southern margin of the Laurentide Ice Sheet, south-central Wisconsin, USA: Implications for cosmogenic dating of glacial terrains, Geological Society of America Bulletin, 114, 1581–1591, https://doi.org/10.1130/0016-7606(2002)114%253C1581:VIGENT%253E2.0.CO;2, 2002.

Collins, C. M., Perdrial, N., Blard, P.-H., Keulen, N., Mahaney, W. C., Mastro, H., Souza, J., Rizzo, D. M., Marrocchi, Y., Knutz, P. C., and Bierman, P. R.: Characterization of the 1966 Camp Century Sub-Glacial Core: A Multiscale Analysis, EGUsphere, 1–33, https://doi.org/10.5194/egusphere-2024-2194, 2024.

Corbett, L. B., Young, N. E., Bierman, P. R., Briner, J. P., Neumann, T. A., Rood, D. H., and Graly, J. A.: Paired bedrock and boulder ^{10}Be concentrations resulting from early Holocene ice retreat near Jakobshavn Isfjord, western Greenland, Quaternary Science Reviews, 30, 1739–1749, https://doi.org/10.1016/j.quascirev.2011.04.001, 2011.

Corbett, L. B., Bierman, P. R., and Rood, D. H.: An approach for optimizing in situ cosmogenic ^{10}Be sample preparation, Quaternary Geochronology, 33, 24–34, https://doi.org/10.1016/j.quageo.2016.02.001, 2016a.

Corbett, L. B., Bierman, P. R., and Rood, D. H.: Constraining multi-stage exposure-burial scenarios for boulders preserved beneath cold-based glacial ice in Thule, northwest Greenland, Earth and Planetary Science Letters, 440, 147–157, https://doi.org/10.1016/j.epsl.2016.02.004, 2016b.

Corbett, L. B., Bierman, P. R., and Davis, P. T.: Glacial history and landscape evolution of southern Cumberland Peninsula, Baffin Island, Canada, constrained by cosmogenic^{10} Be and^{26} Al, Geological Society of America Bulletin, 128, 1173–1192, https://doi.org/10.1130/B31402.1, 2016c.

Corbett, L. B., Bierman, P. R., Rood, D. H., Caffee, M. W., Lifton, N. A., and Woodruff, T. E.: Cosmogenic ^{26}Al/ ^{10}Be surface production ratio in Greenland, Geophysical Research Letters, 44, 1350–1359, https://doi.org/10.1002/2016GL071276, 2017.

Corbett, L. B., Bierman, P. R., Wright, S. F., Shakun, J. D., Davis, P. T., Goehring, B. M., Halsted, C. T., Koester, A. J., Caffee, M. W., and Zimmerman, S. R.: Analysis of multiple cosmogenic nuclides constrains Laurentide Ice Sheet history and process on Mt. Mansfield, Vermont's highest peak, Quaternary Science Reviews, 205, 234–246, https://doi.org/10.1016/j.quascirev.2018.12.014, 2019.

Corbett, L. B., Bierman, P. R., Neumann, T. A., Graly, J. A., Shakun, J. D., Goehring, B. M., Hidy, A. J., and Caffee, M. W.: Measuring multiple cosmogenic nuclides in glacial cobbles sheds light on Greenland

Ice Sheet processes, Earth and Planetary Science Letters, 554, 116673, https://doi.org/10.1016/j.epsl.2020.116673, 2021.

Couette, P., Ghienne, J., Lajeunesse, P., and Van Der Woerd, J.: Climatic control on the retreat of the Laurentide Ice Sheet margin in easternmost Québec–Labrador (Canada) revealed by cosmogenic nuclide exposure dating, J Quaternary Science, 38, 1044–1061, https://doi.org/10.1002/jqs.3525, 2023.

Cowton, T., Nienow, P., Bartholomew, I., Sole, A., and Mair, D.: Rapid erosion beneath the Greenland ice sheet, Geology, 40, 343–346, https://doi.org/10.1130/G32687.1, 2012.

Dalton, A. S., Finkelstein, S. A., Forman, S. L., Barnett, P. J., Pico, T., and Mitrovica, J. X.: Was the Laurentide Ice Sheet significantly reduced during Marine Isotope Stage 3?, Geology, 47, 111–114, https://doi.org/10.1130/G45335.1, 2019.

Dalton, A. S., Margold, M., Stokes, C. R., Tarasov, L., Dyke, A. S., Adams, R. S., Allard, S., Arends, H. E., Atkinson, N., Attig, J. W., Barnett, P. J., Barnett, R. L., Batterson, M., Bernatchez, P., Borns, H. W., Breckenridge, A., Briner, J. P., Brouard, E., Campbell, J. E., Carlson, A. E., Clague, J. J., Curry, B. B., Daigneault, R.-A., Dubé-Loubert, H., Easterbrook, D. J., Franzi, D. A., Friedrich, H. G., Funder, S., Gauthier, M. S., Gowan, A. S., Harris, K. L., Hétu, B., Hooyer, T. S., Jennings, C. E., Johnson, M. D., Kehew, A. E., Kelley, S. E., Kerr, D., King, E. L., Kjeldsen, K. K., Knaeble, A. R., Lajeunesse, P., Lakeman, T. R., Lamothe, M., Larson, P., Lavoie, M., Loope, H. M., Lowell, T. V., Lusardi, B. A., Manz, L., McMartin, I., Nixon, F. C., Occhietti, S., Parkhill, M. A., Piper, D. J. W., Pronk, A. G., Richard, P. J. H., Ridge, J. C., Ross, M., Roy, M., Seaman, A., Shaw, J., Stea, R. R., Teller, J. T., Thompson, W. B., Thorleifson, L. H., Utting, D. J., Veillette, J. J., Ward, B. C., Weddle, T. K., and Wright, H. E.: An updated radiocarbon-based ice margin chronology for the last deglaciation of the North American Ice Sheet Complex, Quaternary Science Reviews, 234, 106223, https://doi.org/10.1016/j.quascirev.2020.106223, 2020.

Dalton, A. S., Stokes, C. R., and Batchelor, C. L.: Evolution of the Laurentide and Innuitian ice sheets prior to the Last Glacial Maximum (115 ka to 25 ka), Earth-Science Reviews, 224, 103875, https://doi.org/10.1016/j.earscirev.2021.103875, 2022.

Dalton, A. S., Dulfer, H. E., Margold, M., Heyman, J., Clague, J. J., Froese, D. G., Gauthier, M. S., Hughes, A. L. C., Jennings, C. E., Norris, S. L., and Stoker, B. J.: Deglaciation of the North American ice sheet complex in calendar years based on a comprehensive database of chronological data: NADI-1, Quaternary Science Reviews, 321, 108345, https://doi.org/10.1016/j.quascirev.2023.108345, 2023.

Davis, P. T., Bierman, P. R., Corbett, L. B., and Finkel, R. C.: Cosmogenic exposure age evidence for rapid Laurentide deglaciation of the Katahdin area, west-central Maine, USA, 16 to 15 ka, Quaternary Science Reviews, 116, 95–105, https://doi.org/10.1016/j.quascirev.2015.03.021, 2015.

Dethier, D. P., Racela, J., and Wieman, S. T.: A contemporary mass-balance approach to small-catchment denudation rates in glaciated New England, GSA Annual Meeting in Indianapolis, Indiana, USA - 2018, 319718, https://doi.org/10.1130/abs/2018AM-319718, 2018.

Dubé-Loubert, H., Roy, M., Schaefer, J. M., and Clark, P. U.: 10Be dating of former glacial Lake Naskaupi (Québec-Labrador) and timing of its discharges during the last deglaciation, Quaternary Science Reviews, 191, 31–40, https://doi.org/10.1016/j.quascirev.2018.05.008, 2018.

Dubé-Loubert, H., Roy, M., Veillette, J. J., Brouard, E., Schaefer, J. M., and Wittmann, H.: The role of glacial dynamics in the development of ice divides and the Horseshoe Intersection Zone of the

northeastern Labrador Sector of the Laurentide Ice Sheet, Geomorphology, 387, 107777, https://doi.org/10.1016/j.geomorph.2021.107777, 2021.

Dyke, A. S.: An outline of North American deglaciation with emphasis on central and northern Canada, in: Developments in Quaternary Sciences, vol. 2, Elsevier, 373–424, https://doi.org/10.1016/S1571-0866(04)80209-4, 2004.

Fame, M. L., Owen, L. A., Spotila, J. A., Dortch, J. M., and Caffee, M. W.: Tracking paraglacial sediment with cosmogenic 10Be using an example from the northwest Scottish Highlands, Quaternary Science Reviews, 182, 20–36, https://doi.org/10.1016/j.quascirev.2017.12.017, 2018.

Ganti, V., Von Hagke, C., Scherler, D., Lamb, M. P., Fischer, W. W., and Avouac, J.-P.: Time scale bias in erosion rates of glaciated landscapes, Sci. Adv., 2, e1600204, https://doi.org/10.1126/sciadv.1600204, 2016.

Gauthier, M. S., Hodder, T. J., Dalton, A. S., Brewer, V., Lian, O. B., Finkelstein, S. A., Schaarschmidt, M., and Mereghetti, A.: South-central Laurentide Ice Sheet dynamics and the formation of proglacial Lake Vita during MIS 3, Quat. res., 1–23, https://doi.org/10.1017/qua.2024.34, 2024.

Goehring, B. M., Kelly, M. A., Schaefer, J. M., Finkel, R. C., and Lowell, T. V.: Dating of raised marine and lacustrine deposits in east Greenland using beryllium−10 depth profiles and implications for estimates of subglacial erosion, J Quaternary Science, 25, 865–874, https://doi.org/10.1002/jqs.1380, 2010.

Goldthwait, J. W. and Kruger, F. C.: Weathered rock in and under the drift in New Hampshire, Geological Society of America Bulletin, 49, 1183–1198, https://doi.org/10.1130/GSAB-49-1183, 1938.

Granger, D. E.: Cosmogenic Nuclide Burial Dating in Archaeology and Paleoanthropology, in: Treatise on Geochemistry, Elsevier, 81–97, https://doi.org/10.1016/B978-0-08-095975-7.01208-0, 2014.

Granger, D. E. and Muzikar, P. F.: Dating sediment burial with in situ-produced cosmogenic nuclides: theory, techniques, and limitations, Earth and Planetary Science Letters, 188, 269–281, https://doi.org/10.1016/S0012-821X(01)00309-0, 2001.

Hallet, B., Hunter, L., and Bogen, J.: Rates of erosion and sediment evacuation by glaciers: A review of field data and their implications, Global and Planetary Change, 12, 213–235, https://doi.org/10.1016/0921-8181(95)00021-6, 1996.

Halsted, C. T., Bierman, P. R., Shakun, J. D., Davis, P. T., Corbett, L. B., Drebber, J. S., and Ridge, J. C.: A critical re−analysis of constraints on the timing and rate of Laurentide Ice Sheet recession in the northeastern United States, J Quaternary Science, 39, 54–69, https://doi.org/10.1002/jqs.3563, 2024.

Heisinger, B., Lal, D., Jull, A. J. T., Kubik, P., Ivy-Ochs, S., Knie, K., and Nolte, E.: Production of selected cosmogenic radionuclides by muons: 2. Capture of negative muons, Earth and Planetary Science Letters, 200, 357–369, https://doi.org/10.1016/S0012-821X(02)00641-6, 2002.

Heyman, J., Stroeven, A. P., Harbor, J. M., and Caffee, M. W.: Too young or too old: Evaluating cosmogenic exposure dating based on an analysis of compiled boulder exposure ages, Earth and Planetary Science Letters, 302, 71–80, https://doi.org/10.1016/j.epsl.2010.11.040, 2011.

Hildes, D. H. D., Clarke, G. K. C., Flowers, G. E., and Marshall, S. J.: Subglacial erosion and englacial sediment transport modelled for North American ice sheets, Quaternary Science Reviews, 23, 409–430, https://doi.org/10.1016/j.quascirev.2003.06.005, 2004.

Hodder, T. J., Gauthier, M. S., Ross, M., and Lian, O. B.: Was there a nonglacial episode in the western Hudson Bay Lowland during Marine Isotope Stage 3?, Quat. res., 116, 148–161, https://doi.org/10.1017/qua.2023.35, 2023.

Hodder, T. J., Gauthier, M. S., Ross, M., Kelley, S. E., Lian, O. B., Dalton, A. S., and Finkelstein, S. A.: Unravelling the fragmented sediment–landform assemblage in an area of thick Quaternary sediment, western Hudson Bay Lowland, Canada, Can. J. Earth Sci., 61, 1156–1183, https://doi.org/10.1139/cjes-2024-0018, 2024.

Hynes, A. and Rivers, T.: Protracted continental collision — evidence from the Grenville Orogen *Lithoprobe — parameters, processes, and the evolution of a continent* ., Can. J. Earth Sci., 47, 591–620, https://doi.org/10.1139/E10-003, 2010.

Jansen, J. D., Knudsen, M. F., Andersen, J. L., Heyman, J., and Egholm, D. L.: Erosion rates in Fennoscandia during the past million years, Quaternary Science Reviews, 207, 37–48, https://doi.org/10.1016/j.quascirev.2019.01.010, 2019.

Jones, R. S., Whitehouse, P. L., Bentley, M. J., Small, D., and Dalton, A. S.: Impact of glacial isostatic adjustment on cosmogenic surface-exposure dating, Quaternary Science Reviews, 212, 206–212, https://doi.org/10.1016/j.quascirev.2019.03.012, 2019.

Klein, J., Giegengack, R., Middleton, R., Sharma, P., Underwood, J. R., and Weeks, R. A.: Revealing Histories of Exposure Using *In Situ* Produced ^{26}Al and^{10}Be in Libyan Desert Glass, Radiocarbon, 28, 547–555, https://doi.org/10.1017/S0033822200007700, 1986.

Koester, A. J., Shakun, J. D., Bierman, P. R., Davis, P. T., Corbett, L. B., Goehring, B. M., Vickers, A. C., and Zimmerman, S. R.: Laurentide ice sheet thinning and erosive regimes at Mount Washington, New Hampshire, inferred from multiple cosmogenic nuclides, in: Untangling the Quaternary Period—A Legacy of Stephen C. Porter, edited by: Waitt, R. B., Thackray, G. D., and Gillespie, A. R., Geological Society of America, 299–314, https://doi.org/10.1130/2020.2548(15), 2021.

Kohl, C. P. and Nishiizumi, K.: Chemical isolation of quartz for measurement of in-situ -produced cosmogenic nuclides, Geochimica et Cosmochimica Acta, 56, 3583–3587, https://doi.org/10.1016/0016-7037(92)90401-4, 1992.

Koppes, M., Hallet, B., Rignot, E., Mouginot, J., Wellner, J. S., and Boldt, K.: Observed latitudinal variations in erosion as a function of glacier dynamics, Nature, 526, 100–103, https://doi.org/10.1038/nature15385, 2015.

Lajeunesse, P. and Allard, M.: Late Quaternary Deglaciation, Glaciomarine Sedimentation and Glacioisostatic Recovery in the Rivière Nastapoka Area, Eastern Hudson Bay, Northern Québec, Géographie physique et Quaternaire, 57, 65–83, https://doi.org/10.7202/010331ar, 2005.

Larue, F., Royer, A., De Sève, D., Langlois, A., Roy, A., and Brucker, L.: Validation of GlobSnow-2 snow water equivalent over Eastern Canada, Remote Sensing of Environment, 194, 264–277, https://doi.org/10.1016/j.rse.2017.03.027, 2017.

LaSalle, P., De Kimpe, C. R., and Laverdiere, M. R.: Sub-till saprolites in southeastern Quebec and adjacent New England: Erosional, stratigraphic, and climatic significance, in: Geological Society of America Special Papers, vol. 197, Geological Society of America, 13–20, https://doi.org/10.1130/SPE197-p13, 1985.

Lavoie, C., Allard, M., and Duhamel, D.: Deglaciation landforms and C-14 chronology of the Lac Guillaume-Delisle area, eastern Hudson Bay: A report on field evidence, Geomorphology, 159–160, 142–155, https://doi.org/10.1016/j.geomorph.2012.03.015, 2012.

LeBlanc, D. E., Shakun, J. D., Corbett, L. B., Bierman, P. R., Caffee, M. W., and Hidy, A. J.: Laurentide Ice Sheet persistence during Pleistocene interglacials, Geology, 51, 496–499, https://doi.org/10.1130/G50820.1, 2023.

Lefebvre−Fortier, C., Roy, M., Dubé−Loubert, H., Brouard, E., and Schaefer, J. M.: Configuration and timing of the postglacial marine incursion along the eastern Ungava Peninsula (Nunavik, Canada): implications for deglaciation models, J Quaternary Science, 39, 359–372, https://doi.org/10.1002/jqs.3591, 2024.

Lifton, N., Sato, T., and Dunai, T. J.: Scaling in situ cosmogenic nuclide production rates using analytical approximations to atmospheric cosmic-ray fluxes, Earth and Planetary Science Letters, 386, 149–160, https://doi.org/10.1016/j.epsl.2013.10.052, 2014.

Liverman, D. G. E.: Quaternary geology of the Goose Bay area:, Current Research. Department of Mines and Energy, Geological Survey, Newfoundland and Labrador, Report, 1997.

Margold, M., Stokes, C. R., and Clark, C. D.: Reconciling records of ice streaming and ice margin retreat to produce a palaeogeographic reconstruction of the deglaciation of the Laurentide Ice Sheet, Quaternary Science Reviews, 189, 1–30, https://doi.org/10.1016/j.quascirev.2018.03.013, 2018.

Marquette, G. C., Gray, J. T., Gosse, J. C., Courchesne, F., Stockli, L., Macpherson, G., and Finkel, R.: Felsenmeer persistence under non-erosive ice in the Torngat and Kaumajet mountains, Quebec and Labrador, as determined by soil weathering and cosmogenic nuclide exposure dating, Can. J. Earth Sci., 41, 19–38, https://doi.org/10.1139/e03-072, 2004.

Marsella, K. A., Bierman, P. R., Davis, P. T., and Caffee, M. W.: Cosmogenic ^{10}Be and ^{26}Al ages for the Last Glacial Maximum, eastern Baffin Island, Arctic Canada, Geological Society of America Bulletin, 112, 1296–1312, https://doi.org/10.1130/0016-7606(2000)112%253C1296:CBAAAF%253E2.0.CO;2, 2000.

Melanson, A., Bell, T., and Tarasov, L.: Numerical modelling of subglacial erosion and sediment transport and its application to the North American ice sheets over the Last Glacial cycle, Quaternary Science Reviews, 68, 154–174, https://doi.org/10.1016/j.quascirev.2013.02.017, 2013.

Merchel, S. and Bremser, W.: First international 26Al interlaboratory comparison – Part I, Nuclear Instruments and Methods in Physics Research Section B: Beam Interactions with Materials and Atoms, 223–224, 393–400, https://doi.org/10.1016/j.nimb.2004.04.076, 2004.

Miller, G., Briner, J., Lifton, N., and Finkel, R.: Limited ice-sheet erosion and complex exposure histories derived from in situ cosmogenic ^{10}Be, ^{26}Al, and ^{14}C on Baffin Island, Arctic Canada, Quaternary Geochronology, 1, 74–85, https://doi.org/10.1016/j.quageo.2006.06.011, 2006.

Miller, G. H. and Andrews, J. T.: Hudson Bay was not deglaciated during MIS-3, Quaternary Science Reviews, 225, 105944, https://doi.org/10.1016/j.quascirev.2019.105944, 2019.

Miller, G. H., Wolfe, A. P., Axford, Y., Briner, J. P., Bueltmann, H., Crump, S., Francis, D., Fréchette, B., Gorbey, D., Kelly, M., McFarlin, J., Osterberg, E., Raberg, J., Raynolds, M., Sepúlveda, J., Thomas, E., and De Wet, G.: Last interglacial lake sediments preserved beneath Laurentide and Greenland Ice sheets provide insights into Arctic climate amplification and constrain 130 ka of ice−sheet history, J Quaternary Science, 37, 979–1005, https://doi.org/10.1002/jqs.3433, 2022.

Nelson, A. H., Bierman, P. R., Shakun, J. D., and Rood, D. H.: Using *in situ* cosmogenic ^{10}Be to identify the source of sediment leaving Greenland, Earth Surf. Process. Landforms, 39, 1087–1100, https://doi.org/10.1002/esp.3565, 2014.

Nishiizumi, K.: Preparation of ^{26}Al AMS standards, Nuclear Instruments and Methods in Physics Research Section B: Beam Interactions with Materials and Atoms, 223–224, 388–392, https://doi.org/10.1016/j.nimb.2004.04.075, 2004.

Nishiizumi, K., Imamura, M., Caffee, M. W., Southon, J. R., Finkel, R. C., and McAninch, J.: Absolute calibration of ^{10}Be AMS standards, Nuclear Instruments and Methods in Physics Research Section B: Beam Interactions with Materials and Atoms, 258, 403–413, https://doi.org/10.1016/j.nimb.2007.01.297, 2007.

Occhietti, S., Parent, M., Lajeunesse, P., Robert, F., and Govare, É.: Late Pleistocene–Early Holocene Decay of the Laurentide Ice Sheet in Québec–Labrador, in: Developments in Quaternary Sciences, vol. 15, Elsevier, 601–630, https://doi.org/10.1016/B978-0-444-53447-7.00047-7, 2011.

Patton, H., Hubbard, A., Heyman, J., Alexandropoulou, N., Lasabuda, A. P. E., Stroeven, A. P., Hall, A. M., Winsborrow, M., Sugden, D. E., Kleman, J., and Andreassen, K.: The extreme yet transient nature of glacial erosion, Nat Commun, 13, 7377, https://doi.org/10.1038/s41467-022-35072-0, 2022.

Patton, H., Alexandropoulou, N., Lasabuda, A. P. E., Knies, J., Andreassen, K., Winsborrow, M., Laberg, J. S., and Hubbard, A.: Glacial erosion and Quaternary landscape development of the Eurasian Arctic, Earth-Science Reviews, 258, 104936, https://doi.org/10.1016/j.earscirev.2024.104936, 2024.

Payette, S., Morneau, C., Sirois, L., and Desponts, M.: Recent Fire History of the Northern Quebec Biomes, Ecology, 70, 656–673, https://doi.org/10.2307/1940217, 1989.

Pelletier, J. D., Broxton, P. D., Hazenburg, P., Zenf, X., Troch, P. A., Niu, G., Williams, Z. C., Brunke, M. A., and Gochis, D.: Global 1-km Gridded Thickness of Soil, Regolith, and Sedimentary Deposit Layers, https://doi.org/10.3334/ORNLDAAC/1304, 2016.

Peteet, D. M., Beh, M., Orr, C., Kurdyla, D., Nichols, J., and Guilderson, T.: Delayed deglaciation or extreme Arctic conditions 21−16 cal. kyr at southeastern Laurentide Ice Sheet margin?, Geophysical Research Letters, 39, 2012GL051884, https://doi.org/10.1029/2012GL051884, 2012.

Pico, T., Birch, L., Weisenberg, J., and Mitrovica, J. X.: Refining the Laurentide Ice Sheet at Marine Isotope Stage 3: A data-based approach combining glacial isostatic simulations with a dynamic ice model, Quaternary Science Reviews, 195, 171–179, https://doi.org/10.1016/j.quascirev.2018.07.023, 2018.

Rice, J. M., Ross, M., Paulen, R. C., Kelley, S. E., Briner, J. P., Neudorf, C. M., and Lian, O. B.: Refining the ice flow chronology and subglacial dynamics across the migrating Labrador Divide of the Laurentide Ice Sheet with age constraints on deglaciation, J Quaternary Science, 34, 519–535, https://doi.org/10.1002/jqs.3138, 2019.

Rice, J. M., Ross, M., Paulen, R. C., Kelley, S. E., and Briner, J. P.: A GIS−based multi−proxy analysis of the evolution of subglacial dynamics of the Quebec–Labrador ice dome, northeastern Quebec, Canada, Earth Surf Processes Landf, 45, 3155–3177, https://doi.org/10.1002/esp.4957, 2020.

Schaefer, J. M., Finkel, R. C., Balco, G., Alley, R. B., Caffee, M. W., Briner, J. P., Young, N. E., Gow, A. J., and Schwartz, R.: Greenland was nearly ice-free for extended periods during the Pleistocene, Nature, 540, 252–255, https://doi.org/10.1038/nature20146, 2016.

Schildgen, T. F., Phillips, W. M., and Purves, R. S.: Simulation of snow shielding corrections for cosmogenic nuclide surface exposure studies, Geomorphology, 64, 67–85, https://doi.org/10.1016/j.geomorph.2004.05.003, 2005.

Shakun, J. D., Corbett, L. B., Bierman, P. R., Underwood, K., Rizzo, D. M., Zimmerman, S. R., Caffee, M. W., Naish, T., Golledge, N. R., and Hay, C. C.: Minimal East Antarctic Ice Sheet retreat onto land during the past eight million years, Nature, 558, 284–287, https://doi.org/10.1038/s41586-018-0155-6, 2018.

Simms, A. R., Lisiecki, L., Gebbie, G., Whitehouse, P. L., and Clark, J. F.: Balancing the last glacial maximum (LGM) sea-level budget, Quaternary Science Reviews, 205, 143–153, https://doi.org/10.1016/j.quascirev.2018.12.018, 2019.

Staiger, J., Gosse, J., Little, E., Utting, D., Finkel, R., Johnson, J., and Fastook, J.: Glacial erosion and sediment dispersion from detrital cosmogenic nuclide analyses of till, Quaternary Geochronology, 1, 29–42, https://doi.org/10.1016/j.quageo.2006.06.009, 2006.

Staiger, J. K. W., Gosse, J. C., Johnson, J. V., Fastook, J., Gray, J. T., Stockli, D. F., Stockli, L., and Finkel, R.: Quaternary relief generation by polythermal glacier ice, Earth Surf Processes Landf, 30, 1145–1159, https://doi.org/10.1002/esp.1267, 2005.

Stokes, C. R., Tarasov, L., and Dyke, A. S.: Dynamics of the North American Ice Sheet Complex during its inception and build-up to the Last Glacial Maximum, Quaternary Science Reviews, 50, 86–104, https://doi.org/10.1016/j.quascirev.2012.07.009, 2012.

Storrar, R. D., Stokes, C. R., and Evans, D. J. A.: A map of large Canadian eskers from Landsat satellite imagery, Journal of Maps, 9, 456–473, https://doi.org/10.1080/17445647.2013.815591, 2013.

Stroeven, A. P., Fabel, D., Harbor, J., Hättestrand, C., and Kleman, J.: Quantifying the erosional impact of the Fennoscandian Ice Sheet in the Torneträsk–Narvik corridor, northern Sweden, based on cosmogenic radionuclide data, Geografiska Annaler: Series A, Physical Geography, 84, 275–287, https://doi.org/10.1111/j.0435-3676.2002.00182.x, 2002.

Sugden, D. E.: Glacial Erosion by the Laurentide Ice Sheet, J. Glaciol., 20, 367–391, https://doi.org/10.3189/S0022143000013915, 1978.

Tiffney, B. H.: Re-evaluation of the age of the Brandon Lignite (Vermont, USA) based on plant megafossils, Review of Palaeobotany and Palynology, 82, 299–315, https://doi.org/10.1016/0034-6667(94)90081-7, 1994.

Ullman, D. J., Carlson, A. E., Hostetler, S. W., Clark, P. U., Cuzzone, J., Milne, G. A., Winsor, K., and Caffee, M.: Final Laurentide ice-sheet deglaciation and Holocene climate-sea level change, Quaternary Science Reviews, 152, 49–59, https://doi.org/10.1016/j.quascirev.2016.09.014, 2016.

Wilner, J. A., Nordin, B. J., Getraer, A., Gregoire, R. M., Krishna, M., Li, J., Pickell, D. J., Rogers, E. R., McDannell, K. T., Palucis, M. C., and Keller, C.: Limits to timescale dependence in erosion rates: Quantifying glacial and fluvial erosion across timescales, Sci. Adv., 10, eadr2009, https://doi.org/10.1126/sciadv.adr2009, 2024.